J. Fluid Mech. (2012), *vol.* 709, *pp.* 445–489. © Cambridge University Press 2012
doi:10.1017/jfm.2012.343

Collision modelling for the interface-resolved simulation of spherical particles in viscous fluids

Tobias Kempe† and Jochen Fröhlich

Institut für Strömungsmechanik, Technische Universitt Dresden, Dresden, 01062, Germany

(Received 4 May 2011; revised 31 May 2012; accepted 2 July 2012;
first published online 23 August 2012)

The paper presents a model for particle–particle and particle–wall collisions during interface-resolving numerical simulations of particle-laden flows. The accurate modelling of collisions in this framework is challenging due to methodological problems generated by interface approach and contact as well as due to the greatly different time scales involved. To cope with this situation, multiscale modelling approaches are introduced avoiding excessive local grid refinement during surface approach and time step reduction during the surface contact. A new adaptive model for the normal forces in the phase of 'dry contact' is proposed, stretching the collision process in time to match the time step of the fluid solver. This yields a physically sound and robust collision model with modified stiffness and damping determined by an optimization scheme. Furthermore, the model is supplemented with a new approach for modelling the tangential force during oblique collisions which is based on two material parameters: a critical impact angle separating rolling from sliding and the friction coefficient for the sliding motion. The resulting new model is termed the adaptive collision model (ACM). All proposed sub-models only contain physical parameters, and virtually no numerical parameters requiring adjustment or tuning. The new model is implemented in the framework of an immersed boundary method but is applicable with any spatial and temporal discretization. Detailed validation against experimental data was performed so that a general and versatile model for arbitrary collisions of spherical particles in viscous fluids is now available.

Key words: computational methods, multiphase flow, particle/fluid flow

1. Introduction

Particle-laden flows are of considerable interest in a wide range of engineering applications. Their accurate and numerically efficient simulation is of substantial importance for academic research and industrial purposes. Simulations with particles modelled as mass points, i.e. without volume as, for example, used by Hoomans *et al.* (1996), Xu & Yu (1997), Sundaram & Collins (1999) and Yang, York & Broeckx (2008) to name but a few publications, have become standard in recent years. In contrast, the three-dimensional, fully coupled and interface-resolving simulation of flows with a huge number of particles of finite size is still an area of active research. An efficient approach to model this situation is provided by an immersed boundary method (IBM), as originally proposed by Peskin (1977). The basic idea of this approach is to employ a numerically efficient Cartesian grid for the discretization of

† Email address for correspondence: tobias.kempe@tu-dresden.de

https://doi.org/10.1017/jfm.2012.343 Published online by Cambridge University Press

the fluid phase and to represent the immersed fluid–solid interface by surface markers. In order to satisfy the required boundary conditions at the interface additional source terms are used in the momentum equation. The book by Prosperetti & Tryggvason (2007) as well as several review papers (Iaccarino & Verzicco 2003; Mittal & Iaccarino 2005; Uzgoren *et al.* 2007) provide an overview of the different variants of this approach. Particularly focusing on particle-laden suspensions Uhlmann (2005) proposed an efficient IBM for such interface-resolving simulations, treating the flow field as a constant-density field inside and outside the particles so that performance problems of the Poisson solver due to high density ratios are avoided. Extracting the forces on the particles, ordinary differential equations are solved for their trajectories. No empirical correlations are required for the fluid forces since the interface is fully resolved. While this method, in modified form, constitutes the framework of the present study, the goal here is beyond the IBM technique. Collisions involve features on very small time and length scales so that necessarily physical modelling and introduction of empirical information is required at some stage. The purpose of the present paper is to provide such a model for arbitrary collisions in a particle-laden wall-bounded suspension.

In particle-laden flows, particle–particle and particle–wall collisions can occur. Even for low volume fractions particle–wall collisions need to be represented accurately to yield realistic particle concentrations in the flow field (Lain, Sommerfeld & Kussin 2002). For larger volume fractions particle–particle collisions also contribute to the momentum balance of the suspension. The accurate numerical modelling of the collision process hence is crucial for the quality of the simulation in a vast regime of parameters.

Despite the rapid increase of available computer power not all scales of the flow and the collision process itself can be entirely resolved in a typical multiphase flow, since these often span more than two orders of magnitude. During the collision of two particles, for example, a thin lubrication layer is formed between the surfaces and the fluid is squeezed out of this gap when the particles approach and is pushed back into the gap during rebound. This feature might be resolved by an adaptive local grid refinement as proposed e.g. by Hu (1996), but this usually results in substantially increased computation time (Tryggvason *et al.* 2010). A similar problem occurs during the direct contact of the surfaces if the elasticity of the particle is accounted for. Since the ordinary differential equation (ODE) for the particle position during that phase is very stiff, the time step has to be reduced significantly in order to resolve the collision in time. Spatial and temporal grid refinement in the described manner makes a simulation with 10^4 and more particles practically unfeasible.

Particle–particle and particle–wall collisions in viscous fluids have been investigated experimentally in several papers. Among the first was McLaughlin (1968) who released steel spheres to fall freely under gravitation onto a plane steel wall in a glycerine–water solution. He investigated the energy loss resulting from the collision by means of the rebound height of the spheres. Davis, Serayssol & Hinch (1986) developed an elasto-hydrodynamic lubrication theory to couple the interstitial fluid pressure with the solid surface deformation and showed by theoretical considerations that the rebound of the particle after collision depends on the Stokes number based on the impact velocity of the particle. Barnocky & Davis (1988) and Davis, Rager & Good (2002) later performed experiments on particles colliding with a surface coated with a viscous fluid film. Their results show good agreement with the theoretical predictions of Davis *et al.* (1986). Ten Cate *et al.* (2002) and Pianet *et al.* (2007) carried out experiments with spheres of various sizes in a viscous fluid to investigate

https://doi.org/10.1017/jfm.2012.343 Published online by Cambridge University Press

the behaviour of particles moving towards a wall. In these studies the Stokes number was lower than the critical value $St = 10$ and therefore the particles did not rebound from the surface. Gondret *et al.* (1999) and Gondret, Lance & Petit (2002) performed experiments similar to Ten Cate *et al.* (2002) and Pianet *et al.* (2007) but with Stokes numbers higher than the critical value. Trajectories of particles falling at their terminal velocity, impacting on a submerged surface and rebounding from the surface were determined. In these experiments the normal coefficient of restitution clearly was a function of the Stokes number, hence confirming the theoretical results of Davis *et al.* (1986). In the experiments of Zenit & Hunt (1999) and Joseph (Joseph *et al.* 2001; Joseph 2003; Joseph & Hunt 2004) glass and steel spheres of various diameters were fixed at the end of a pendulum and were released to fall freely onto a vertical plane wall in water and glycerol. Joseph *et al.* (2001) investigated only normal particle–wall collisions, which was later extended to oblique particle–wall collisions by Joseph & Hunt (2004).

The limiting case of a collision is obtained when a particle is in continuous contact with a wall or another particle. Experiments on particles rolling down an inclined surface in a viscous fluid were performed by Prokunin & Williams (1996) and Prokunin (1998). These authors found, that at small Reynolds numbers, motion with or without particle–wall contact may occur. Yang *et al.* (2006) investigated the motion of a heavy sphere in a rotating cylinder completely filled with a highly viscous fluid. A vapour bubble below the sphere resulting from cavitation was observed over the entire range of rotation rates. While the models developed in the present paper may be applied for situations with continuous contact as well (Vowinckel, Kempe & Fröhlich 2011) we focus here on proper collisions in the sense that the surface contact is of finite duration.

While the situation in granular media is only to a negligible extent influenced by the gas surrounding the particles due to the low density and low viscosity, the collision process in a viscous fluid also depends on the viscous interaction of the disperse phase with the surrounding fluid. The complex vortex dynamics associated with the collision of a sphere with a solid wall have been investigated by several authors. Among the first were Eames & Dalziel (2000) who experimentally studied the flow around a sphere moving in a normal or oblique direction towards a wall or away from a wall. In their experiments the motion of the sphere was prescribed by the apparatus. It was stopped when the sphere touched the wall so that no rebound from the surface was allowed. Later, Leweke, Thompson & Hourigan (2004, 2006) and Thompson, Leweke & Hourigan (2007) experimentally and numerically studied the instability of the flow around a sphere impacting on a wall. These authors found that a complex vortex ring develops due to the interaction with the wall. At higher Reynolds numbers a non-axisymmetric instability develops, yielding a rapid dispersion of the vortex system.

In contrast to the particle–wall collisions discussed so far, well-resolved experimental data on particle–particle collisions are scarce. In the experiments of Zhang *et al.* (1999) the dynamic behaviour of the collision of two elastic spheres in a stagnant viscous fluid was investigated. A freely moving sphere was released above a fixed sphere for a co-linear collision and the particle trajectories were recorded. The particle Reynolds numbers assumed values from 5 to 300 in that study. The experiments of Yang & Hunt (2006) were conducted with particles fixed at the end of a pendulum string similar to the configuration of Joseph (2003). These particles were released to impact onto another particle which was also fixed to a pendulum. The particle trajectories were measured which allowed the restitution

https://doi.org/10.1017/jfm.2012.343 Published online by Cambridge University Press

coefficient to be determined. Donahue *et al.* (2008) investigated the simultaneous normal collision between three solid spheres in air by means of an experiment inspired by Newton's cradle. An initially touching pair of particles was hit by a third particle and measurements of collision durations and post-collisional velocities were performed. These authors later extended their experiment to the simultaneous collision of three spheres with a liquid coating (Donahue, Hrenya & Davis 2010*a*; Donahue *et al.* 2010*b*). In their so-called Stokes cradle, the post-collisional velocities of the spheres were measured for a range of parameters.

Several numerical models for the collision process between particles and for the collision of particles with walls have been developed in the framework of the discrete-element method (DEM) for granular media (Crowe, Sommerfeld & Tsuji 1998; Crowe 2006) where the hydrodynamic interaction between particles is neglected. This is equivalent to considering infinite Stokes number. These models can be divided into two groups: hard-sphere models and soft-sphere models. The hard-sphere approach (Hoomans *et al.* 1996) is based on binary, quasi-instantaneous collisions. The post-collisional velocities are calculated from momentum conservation between the states before and after surface contact. In the soft-sphere approach the motion of the particles is calculated by numerically integrating the equations of motion of the particles accounting for the forces acting on them. Several experimental and numerical studies dealing with the appropriate modelling of the inter-particle forces with this approach have been published. Kruggel-Emden *et al.* (2007) and Stevens & Hrenya (2005) considered normal force models, while Vu-Quoc, Lesburg & Zhang (2004), Kruggel-Emden, Wirtz & Scherer (2008) and Becker & Briesen (2008) investigated the modelling of tangential forces. Typical for all soft-sphere models is that very small time steps must be used to ensure that for reasons of stability and accuracy the step size in time is smaller than the duration of the contact.

For collisions in viscous fluids various numerical models have been proposed in the literature (Diaz-Goano, Minev & Nandakumar 2003; Ten Cate *et al.* 2004; Apostolou & Hrymak 2008; Ardekani & Rangel 2008; Ardekani, Dabiri & Rangel 2008). Soft-sphere models were employed for the simulation of point particles in viscous media with stiffness fixed to a value lower than obtained with realistic material pairing. Xu & Yu (1997) and Yang *et al.* (2008), for example, used the model of Cundall & Strack (1979) while Apostolou & Hrymak (2008) used the model of Walton (Walton & Braun 1986; Walton 1993).

For interface-resolving simulation of particles in viscous fluids the repulsive potential proposed by Glowinski *et al.* (1999, 2001), for example, has been successfully used in relatively dilute flows (Feng & Michaelides 2005; Uhlmann 2008) where collisions are of minor importance, and also for the simulation of particle transport in a rough-wall turbulent open channel flow (Chan-Braun, García-Villalba, and Uhlmann 2010). This model, however, does not account for energy dissipation during the surface contact, nor for tangential forces, so that collision-induced rotation of spherical particles cannot be captured, for example. Veeramani, Minev & Nandakumar (2009) and Vanella & Balaras (2009) employed a hard-sphere model (HSM) for the surface contact, but these studies lack validation of the collision model with experimental data. In the paper of Ardekani & Rangel (2008), instead of applying a repulsive force between the particles, a contact force is computed from the conservation of linear momentum in the normal and tangential directions. The contact model was applied to normal particle–wall collisions and the resulting numerical coefficient of restitution was found to be in good agreement with experimental data. The effect of Stokes number and surface roughness on the restitution coefficient was

https://doi.org/10.1017/jfm.2012.343 Published online by Cambridge University Press

investigated, but no comparison of the particle trajectories with experimental data was performed. Furthermore, these authors investigated the velocity profiles before and after surface contact in the gap between a spherical particle and the wall. Feng, Michaelides & Mao (2010) used a soft-sphere model (SSM) with a fixed lowered stiffness for the simulation of normal and oblique particle–wall collisions. They investigated the effect of spring stiffnesses in the normal and tangential directions on collision duration and rebound trajectories.

A conclusion from the available literature as well as from our own numerical experiments reported in § 2 below is that the collision models which have been developed in the framework of the DEM cannot simply be transferred to collisions in viscous flow. The purpose of the present paper hence is to supplement the basic IBM with appropriate models for the unresolved fluid scales and to propose a modelling concept which covers normal as well as oblique collisions, with and without particle rotation.

To this end we first illustrate the problems encountered with existing physical and numerical models from the literature. During the present study it turned out that issues of numerical discretization with the basic IBM need to be resolved. This numerical method is the subject of a companion paper and hence only recalled briefly here in § 2.2. In § 3, a new model, the adaptive collision time model (ACTM), is presented in the case of purely normal collisions. Normal collisions of rotating particles and oblique collisions require a model for tangential forces which is developed in § 4. Each modelling step is accompanied by detailed validation by means of experimental data.

2. Failure of existing models

2.1. *Numerical method*

The equations to be solved are the unsteady three-dimensional Navier–Stokes equations for a Newtonian fluid of constant density

$$\frac{\partial \boldsymbol{u}}{\partial t} + \boldsymbol{\nabla} \cdot (\boldsymbol{u}\boldsymbol{u}) = \frac{1}{\rho_f} \boldsymbol{\nabla} \cdot \boldsymbol{\tau} + \boldsymbol{f}, \tag{2.1}$$

$$\boldsymbol{\nabla} \cdot \boldsymbol{u} = 0, \tag{2.2}$$

where $\boldsymbol{\tau}$ is the hydrodynamic stress tensor

$$\boldsymbol{\tau} = -p\boldsymbol{I} + \nu_f \rho_f (\boldsymbol{\nabla}\boldsymbol{u} + (\boldsymbol{\nabla}\boldsymbol{u})^{\mathrm{T}}). \tag{2.3}$$

Nomenclature is as usual, with $\boldsymbol{u} = (u, v, w)^{\mathrm{T}}$ designating the velocity vector in Cartesian components, i.e. along the Cartesian coordinates x, y, z, while p is pressure, ρ_f fluid density, $\boldsymbol{f} = (f_x, f_y, f_z)^{\mathrm{T}}$ specific volume force, $\boldsymbol{I}$ the identity matrix, ν_f kinematic viscosity of the fluid, and t time. The spatial discretization of (2.1)–(2.2) is performed by a second-order finite-volume scheme on a staggered grid (Harlow & Welch 1965). The coupling of the fluid and the solid phase is realized by an IBM according to Uhlmann (2005) which is based on inserting additional volume forces in the vicinity of the interface. The fluid–solid interface is represented by discrete surface markers and the transfer between Eulerian and Lagrangian points is performed by interpolation implemented via a weighted sum of regularized Dirac delta functions. In the present implementation the three-point function of Roma, Peskin & Berger (1999) is used as it provides a good balance between numerical efficiency and smoothing properties. For the distribution of a given number N_L of Lagrangian points on the surface of the sphere, the method of Leopardi (2006) is employed. The time-advancement of (2.1) is accomplished by an explicit third-order low-storage

https://doi.org/10.1017/jfm.2012.343 Published online by Cambridge University Press

Runge–Kutta scheme for the convective terms and a Crank–Nicolson scheme for the viscous terms. The Lagrangian interface force is determined directly at the surface makers by the so-called direct forcing of Mohd-Yusof (1997). The solution of a pressure Poisson equation and projection yields the divergence-free velocity field at the end of the Runge–Kutta step.

The second element of the method is constituted by the equations of motion of the particle. Ordinary differential equations are solved for the translation velocity of the particle and for its angular velocity using the same Runge–Kutta scheme as employed for the fluid solver.

2.2. *Improved numerical method*

In some cases numerical difficulties were observed with the IBM presented above which motivated the development of an enhanced method by means of an improved spatial and temporal discretization scheme. This method is employed here. It is the subject of a companion paper (Kempe & Fröhlich 2012) and for this reason only briefly described in this section.

Compared to the original method, the coupling of solid and fluid phases is strengthened by an additional forcing loop which is performed before the solution of the Poisson equation and hence does not significantly increase the computational effort. The additional forcing substantially improves the imposition of the no-slip condition at the surface of solid bodies. As a result, larger time steps can be used. Even more important is that strong acceleration of particles, characteristic for collision processes, is no longer detrimental to the no-slip condition.

Second, the stability range of the method was significantly increased by the direct integration of the linear and angular momentum of the fluid inside the particle control volume by employing a numerically efficient level-set approach. With this modification, no assumption on the motion of the fluid inside the particle as used in Uhlmann (2005) is required.

If interfaces approach or if they are in direct contact the conditions for spreading of forces from the Lagrangian points on the surfaces to the Eulerian grid points are violated with the basic scheme yielding an inconsistent time scheme. As a remedy all surface marker points are excluded from the computation of forces at surfaces of solid bodies whose stencil overlaps with the stencil of a collision partner. The trajectory of the involved particles is still described correctly by their equations of motion since the collision model provides the correct forces. This improved discretization is used throughout in the following and constitutes the framework for implementation which in the present paper focuses on the physical collision modelling.

2.3. *Results for existing models*

This section aims to illustrate the starting point of the present work by showing the unsolved problems encountered with classical collision models when these are used with the IBM of Uhlmann (2005) or even with the improved IBM of Kempe & Fröhlich (2012) described above. Details of all models will be given in § 3 below. As an example we take the collision of a 3 mm steel sphere in silicone oil RV 10 ($\rho_f = 935$ kg m^{-3}, $\nu_f = 1.0692 \times 10^{-2}$ N s m^{-2}) with a horizontal plane glass wall investigated experimentally by Gondret *et al.* (2002). The Stokes number based on the impact velocity is $St = 152$ and the particle Reynolds number is $Re_p = 165$. The computational domain $\Omega = [0; L_x] \times [0; L_y] \times [0; L_z]$ with $L_x = L_y = L_z = 40$ mm was discretized with $N_x \times N_y \times N_z = 256 \times 256 \times 256$ points. A time step corresponding to a Courant–Friedrichs–Levi number of $CFL = 0.6$ was used in all cases. The spatial

https://doi.org/10.1017/jfm.2012.343 Published online by Cambridge University Press

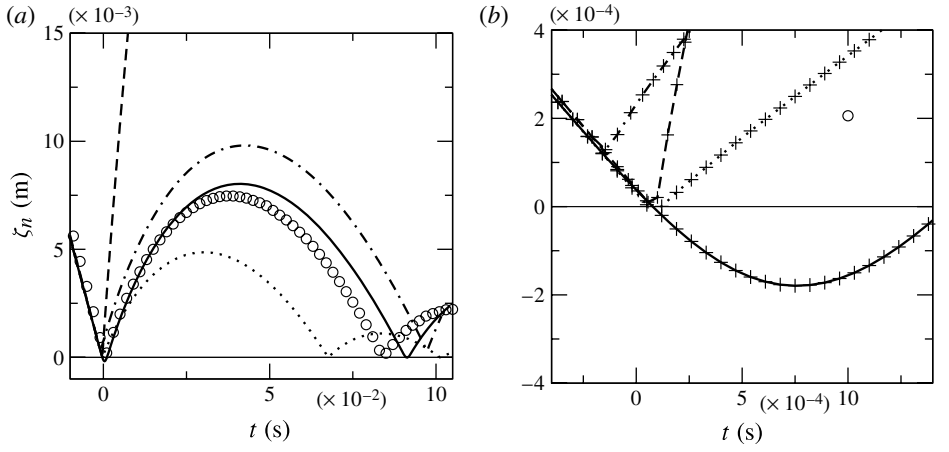


FIGURE 1. Normal impact of a 3 mm steel sphere in silicon oil RV10 on a glass wall for $St = 152$ and $Re = 165$. (*a*) Surface distance ζ_n versus time: ○, Experiment Gondret *et al.* (2002); · · · · · ·, hard-sphere model (HSM), (3.31) below; − − −, soft-sphere model (SSM), (3.15) below; · − · − ·, repulsive potential (RPM), (3.33) below; with $\epsilon^{-1} = 10^2$, ——-, RPM with $\epsilon^{-1} = 10^6$. (*b*) Enlarged view of the time interval around the interface contact, crosses mark data from individual time steps.

resolution of the sphere is $D_p/h \approx 20$, where h is the cell size of the equidistant Cartesian grid and D_p the particle diameter. The surface of the sphere is represented by $N_L = 1159$ marker points.

Three different collision models from the literature are employed here without any modification. First, the so-called HSM according to Foerster *et al.* (1994) is used, described with all details in § 3.4.2 below. The second model is the SSM (Stevens & Hrenya 2005; Kruggel-Emden *et al.* 2007), recalled in § 3.4.3, while the third model is based on a repelling potential model (RPM) as presented by Glowinski *et al.* (1999, 2001) and described in § 3.4.4. The latter is used here with two different values of the stiffness parameter, $\epsilon^{-1} = 10^2$ and $\epsilon^{-1} = 10^6$.

The numerical results for the distance of the surface of the sphere from the wall, ζ_n, versus time are shown in figure 1 with the experimental data included for comparison. All models fail to correctly predict the rebound trajectory of the particle. In the case of the HSM, the surrounding fluid cannot follow the rapid velocity changes of the solid within one time step. This yields an over-prediction of the viscous forces at the particle surface and causes a rapid deceleration of the particle.

The SSM, on the other hand, exhibits the problem of strongly different time scales for the interface contact, τ_c, and for the fluid solver, τ_f. According to the contact theory of Hertz (1882) the collision time is $T_c \approx 1.59 \times 10^{-5}$ s in the present case. For an adequate resolution of the collision process a certain number of time steps are required, for example 10. Since $\tau_c = T_c$ this yields $\Delta t_c = T_c/10 = 1.59 \times 10^{-6}$ s. In figure 1, the time step is not reduced with respect to the step size $\Delta t_f \approx 1 \times 10^{-4}$ s required to resolve τ_f without collision, so that the criterion for accurate time integration of the collision process is violated. Simulations with the SSM at a reduced time step of $\Delta t = 1.59 \times 10^{-6}$ s were undertaken and a realistic trajectory was obtained. If a single particle is to be simulated, a temporal reduction of the time step by a factor of $\Delta t_f/\Delta t_c \approx 63$, for the present case, might be feasible. For simulating a suspension

https://doi.org/10.1017/jfm.2012.343 Published online by Cambridge University Press

with 10^4 or more particles, however, the time step would have to be reduced by this amount almost throughout, which is unfeasible as the computational cost of the simulation then would increase by the same factor. Hence, the failure of the SSM for large time steps is demonstrated here as this would be the regime of its application in suspension flows. As a remedy, Feng *et al.* (2010) and Papista, Dimitrakis & Yiantsios (2011) reduced the stiffness compared to the experimental values in order to allow a larger time step in the simulation. The choice of this parameter, however, is fairly arbitrary, has to be done *a priori*, and depends on the flow.

This drawback is also experienced with the RPM. Figure 1 illustrates that different choices of the stiffness parameter in the RPM yield different trajectories so that it may be a matter of luck to choose an appropriate value. Furthermore, this value would be used throughout in a computed flow where at different times and locations different collision velocities occur.

Comparing the results obtained with the standard IBM (not presented here) and the improved IBM (figure 1) shows that the results for the collision are not significantly enhanced with the new method. Hence, the observed differences between simulation and experiment are indeed an issue of the collision modelling and not related to the discretization method.

3. Modelling of normal collisions

3.1. *Principal approach*

In this section, to begin with, we consider normal collisions and assume non-rotating particles. An appropriate model for this situation is provided here which is later generalized to arbitrary angles and to collisions involving rotating particles. Particle–particle and particle–wall collisions are discussed together as the latter case is obtained by increasing the radius of one of the particles to infinity.

The entire collision process between two particles in a viscous fluid is governed by several physical phenomena and can be decomposed into three phases (Joseph *et al.* 2001). (*a*) The approach phase during which fluid forces govern the interaction. The pressure at the front of the particle increases due to the displacement of the fluid between the particles. When the fluid is squeezed out of the gap viscous forces are generated as well. (*b*) The actual collision takes place when the solid bodies touch. Their deformation, possibly with elastic and plastic contributions, is the dominant mechanism so that this phase is governed by the respective equations for the solid. Since the deformations of the bodies involved are extremely small for typical materials and typical collision parameters this phase is not altered by the presence of the viscous fluid (this will be refined and substantiated in § 3.3.3 below). As illustrated in § 2 above, the phase of direct contact is substantially shorter than characteristic times of the fluid. Most importantly, fluid forces are substantially smaller than the contact forces. This phase of the collision in a viscous fluid hence is equivalent to a collision without surrounding fluid so that the term ‘dry collision’ is used in what follows to designate this phase of the viscous collision. (*c*) The third phase is the rebound phase, again dominated by particle–fluid interaction, similar to the approach phase.

It should be noted that the fluid forces become very large for small gaps, in fact singular if perfectly smooth walls are assumed. Since the step size of the Eulerian grid is finite, fluid forces cannot be resolved for surface distances of the order of or below this step size of the grid. A so-called lubrication model will be used to represent these, hence employed for both phase (*a*) and phase (*c*), when surface distances are

https://doi.org/10.1017/jfm.2012.343 Published online by Cambridge University Press

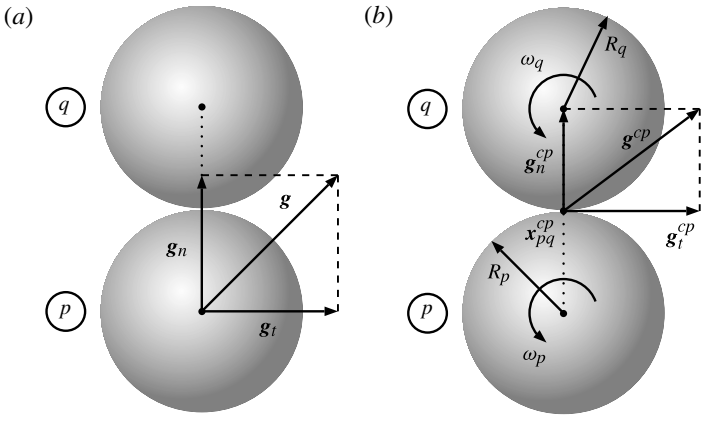


FIGURE 2. Collision of two particles. (*a*) Particle centre relative velocities. (*b*) Sketch of two spherical particles that are in contact at the point $\boldsymbol{x}_{pq}^{cp}$. Relative surface velocity at the contact point in the normal direction is $\boldsymbol{g}_n^{cp}$ and in the tangential direction $\boldsymbol{g}_t^{cp}$. Rotations ω_p and ω_q do not necessarily have to be around collinear axes (cf. (3.6)) but have been drawn like this here for ease of presentation.

small. Fluid forces for larger distances are resolved by the direct computation of the fluid–solid interaction captured by the IBM.

3.2. *Geometry and nomenclature*

The geometric and kinematic data for the collision of two spherical particles p and q are displayed in figure 2. Two different situations have to be considered. For the normal part of the collision process, i.e. the contribution due to approach along the line through the two centres without rotation, only the relative velocity of the centre of mass of the particles is of interest, which is shown in figure 2(*a*). For oblique collisions tangential forces have to be accounted for as well. In the case of vanishing distance between the two surfaces (figure 2*b*) the definition of the contact point $\boldsymbol{x}_{pq}^{cp}$ is obvious. If the minimal surface distance is larger than zero, a virtual contact point $\boldsymbol{x}_{pq}^{cp}$ on both particle surfaces is defined as the point on the surface with the closest distance to the neighbouring particle. If according to some model the surfaces are allowed to slightly penetrate each other, the contact point is defined as the mean of the points of intersection of the connection of the centres of mass with the two surfaces.

In the following, we present some geometrical quantities required for the later study and fix the notation. The unit vector from particle p to particle q is

$$\boldsymbol{n}_{pq} = \frac{\boldsymbol{x}_q - \boldsymbol{x}_p}{|\boldsymbol{x}_q - \boldsymbol{x}_p|}, \tag{3.1}$$

where $\boldsymbol{x}_p$ is the centre of mass of particle p and $\boldsymbol{x}_q$ the centre of mass of particle q. The relative velocity of the particle centres is given by

$$\boldsymbol{g}_{pq} = \boldsymbol{u}_p - \boldsymbol{u}_q, \tag{3.2}$$

where $\boldsymbol{u}_p$ is the velocity of the centre of mass of particle p. The relative normal velocity then is

$$g_{n,pq} = \boldsymbol{g}_{pq} \cdot \boldsymbol{n}_{pq}, \tag{3.3}$$

https://doi.org/10.1017/jfm.2012.343 Published online by Cambridge University Press

and the relative velocity vector of the particle centres in the normal direction is

$$\boldsymbol{g}_{n,pq} = g_{n,pq}\boldsymbol{n}_{pq}, \tag{3.4}$$

so that the relative velocity of the particle centres in the tangential direction is

$$\boldsymbol{g}_{t,pq} = \boldsymbol{g}_{pq} - \boldsymbol{g}_{n,pq}. \tag{3.5}$$

The relative velocity of the surfaces of the particles at the contact point $\boldsymbol{x}_{pq}^{cp}$ hence is

$$\boldsymbol{g}_{pq}^{cp} = \boldsymbol{g}_{pq} + R_p(\boldsymbol{\omega}_p \times \boldsymbol{n}_{pq}) - R_q(\boldsymbol{\omega}_q \times \boldsymbol{n}_{qp}), \tag{3.6}$$

where R_p is the radius of particle p. For spherical particles where the contact point lies on the line through the centres of mass one has

$$\boldsymbol{g}_{n,pq}^{cp} = \boldsymbol{g}_{n,pq}, \tag{3.7}$$

and hence the tangential relative surface velocity at the contact point is given by

$$\boldsymbol{g}_{t,pq}^{cp} = \boldsymbol{g}_{pq}^{cp} - \boldsymbol{g}_{n,pq}. \tag{3.8}$$

The unit vector at the contact point in the tangential direction is defined by

$$\boldsymbol{t}_{pq}^{cp} = \frac{\boldsymbol{g}_{t,pq}^{cp}}{g_{t,pq}^{cp}}, \tag{3.9}$$

where

$$g_{t,pq}^{cp} = |\boldsymbol{g}_{t,pq}^{cp}|. \tag{3.10}$$

The singularity in (3.9) for $g_{t,pq}^{cp} = 0$ is avoided numerically by adding a small number to the denominator. The normal distance between the surfaces of colliding spherical particles p and q is given by

$$\zeta_{n,pq} = |\boldsymbol{x}_q - \boldsymbol{x}_p| - (R_p + R_q). \tag{3.11}$$

For collisions of a particle with a plane wall the distance between the surfaces is

$$\zeta_{n,pw} = (\boldsymbol{x}_p - \boldsymbol{x}_w) \cdot \boldsymbol{n}_w - R_p, \tag{3.12}$$

with $\boldsymbol{n}_w$ the normal vector of the wall pointing into the fluid domain and $\boldsymbol{x}_w$ an arbitrary point on the wall. If $\zeta_n < 0$, the two bodies involved overlap.

3.3. *Physical modelling*

For three-dimensional systems with a large number of particles, such as highly loaded suspensions in large domains, a micro-scale modelling of collisions employing the governing equations of elasticity would be beyond our focus and far too costly even on high-performance computers. Therefore, a macroscopic description of the collision process is needed. In this section we first treat the normal forces.

According to the discussion in § 3.1 the force $\boldsymbol{F}_p$ on a particle p to be modelled during the collision process can be decomposed as

$$\boldsymbol{F}_p = \sum_{q,q\neq p}^{N_p} \left(\boldsymbol{F}_{n,pq}^{lub} + \boldsymbol{F}_{n,pq}^{col} + \boldsymbol{F}_{t,pq}^{col} \right), \tag{3.13}$$

where $\boldsymbol{F}_n^{col}$ is the normal and $\boldsymbol{F}_t^{col}$ the tangential force during the interface contact, while $\boldsymbol{F}^{lub}$ is the modelled lubrication force during approach and rebound. The

https://doi.org/10.1017/jfm.2012.343 Published online by Cambridge University Press

torque $\boldsymbol{M}_p$ on a spherical particle p generated by the tangential contact forces is

$$\boldsymbol{M}_p = \sum_{q,q\neq p}^{N_p} R_p \boldsymbol{n}_{pq} \times \left(\boldsymbol{F}_{t,pq}^{lub} + \boldsymbol{F}_{t,pq}^{col}\right). \tag{3.14}$$

Collision modelling now amounts to providing suitable expressions for the normal and tangential forces introduced in (3.13) and (3.14).

3.3.1. *Dry collisions*

Dry normal collisions of spherical particles can be described by a force–displacement law as provided for example by the contact theory of Hertz (1882). Hertz solved the linear elasticity equation for elastic bodies in contact. In technically relevant cases the contact time is long compared to the lowest mode of vibration of the two spheres (Timoshenko & Goodier 1970). Therefore, the treatment of the collision of two elastic bodies is based on the assumption that the stress system in the vicinity of the region of contact may be determined from equilibrium of stresses, i.e. by neglecting inertial or stress wave effects. The final quasi-static relation between force and displacement for the interface contact is (Hertz 1882)

$$F_n^{col} = k_n \left(-\zeta_n\right)^{3/2}. \tag{3.15}$$

In that equation, the material stiffness k_n is given by

$$k_n = \frac{4}{3}\sqrt{\frac{R_p R_q}{R_p + R_q}}\left(\frac{1-\nu_p^2}{E_p} + \frac{1-\nu_q^2}{E_q}\right)^{-1}, \tag{3.16}$$

for the collision of particles p and q, where E is the Young modulus and ν the Poisson ratio.

To determine the collision time T_c, Hertz solved the equation of motion based on the relative velocity of the particles, $g_{n,pq}$. The impact velocity u_{in} and the rebound velocity u_{out} of the particles are defined by

$$u_{in} = g_{n,pq} \quad (\zeta_n = 0, t = 0), \tag{3.17}$$

and

$$u_{out} = g_{n,pq} \quad (\zeta_n = 0, t = T_c), \tag{3.18}$$

respectively. The contact time for a dry collision according to this theory then is given by

$$T_{c,H} = \frac{2\sqrt{\pi}\Gamma\left(\frac{7}{5}\right)}{\Gamma\left(\frac{9}{10}\right)}\left(\frac{5}{4}\frac{m_p m_q}{k_n(m_p+m_q)}\right)^{2/5} u_{in}^{-1/5} \approx 3.218\left(\frac{m_p m_q}{k_n(m_p+m_q)}\right)^{2/5} u_{in}^{-1/5}, \tag{3.19}$$

where Γ is the Euler Gamma function, evaluated to obtain the approximation on the right-hand side. The collision time of a dry particle–wall collision is found for $m_q \to \infty$. In both cases, particle–particle collision and particle–wall collision, the duration of the contact is proportional to the radius of the sphere and inversely proportional to $u_{in}^{1/5}$. This result has been verified in several experiments such as the one of Stevens & Hrenya (2005). According to the theory, the maximum surface penetration during collisions, $-\zeta_{n,H}^{min}$, then is

$$-\zeta_{n,H}^{min} = 1.093\left(\frac{m_p m_q}{k_n(m_p+m_q)}\right)^{2/5} u_{in}^{4/5}. \tag{3.20}$$

https://doi.org/10.1017/jfm.2012.343 Published online by Cambridge University Press

During the impact of an elastic sphere on an elastic wall some of the kinetic energy is radiated into the wall in the form of elastic waves and is not available for subsequent recovery in the form of kinetic energy after rebound. This loss determines the maximum possible value of the coefficient of restitution for any impact. The coefficient of restitution for dry collisions is defined as the ratio of rebound velocity to impact velocity without any fluid:

$$e_{dry} = -\frac{u_{out}}{u_{in}}. \tag{3.21}$$

In the contact theory of Hertz the material damping is neglected, hence $e_{dry} = 1$ in all cases. Hunter (1957) and Reed (1985) therefore extended the analysis of Hertz to account for the energy loss by elastic waves during the impact and the resulting restitution coefficients compare fairly well with experimental data.

3.3.2. *Restitution coefficient in viscous fluids*

In viscous media, the hydrodynamic forces during approach and rebound have to be accounted for. Hence, a coefficient of restitution for collisions in viscous media, e, is introduced which provides a global description of the rebound. It includes the hydrodynamic interactions of the collision partners as well as the material damping during the dry interface contact and is defined by

$$e = -\frac{u_{out,0}}{u_{in,0}}, \tag{3.22}$$

where $u_{in,0}$ is the particle velocity at a distance $\zeta_{n,0}$, large enough to neglect hydrodynamic interactions of the particle with the wall, and $u_{out,0}$ is the rebound velocity at position $\zeta_{n,0}$ again, after rebound.

The theoretical and experimental findings of Davis *et al.* (1986) and Barnocky & Davis (1988) demonstrate that e is not a function of the Reynolds number Re_p only. Instead, e depends on the Stokes number

$$St = \frac{\rho_p D_p u_p}{9\nu_f \rho_f} = \frac{\rho_p}{9\rho_f} Re_p, \tag{3.23}$$

which is the ratio of the hydrodynamic response time of the particle to a characteristic flow time here taken at $\zeta_{n,0}$. Comments on the practical determination of $\zeta_{n,0}$ which is not a constant value (Joseph *et al.* 2001), will be made below.

For larger Stokes numbers the influence of viscous forces on the particle motion becomes smaller, so that in the limit $St \to \infty$, simultaneously $e \to e_{dry}$. This was indeed observed in the experiments of Gondret *et al.* (1999, 2002) as displayed by the symbols in figure 7(*b*) below. For $St \leqslant 10$, substantial energy is dissipated due to the lubrication forces during the approach so that no rebound of the particle is observed in this regime.

3.3.3. *Collision time in viscous fluids*

Based on the particle–wall collision experiments of Zenit & Hunt (1999), a simple correlation was proposed by Legendre *et al.* (2006) to account for the effects of the fluid inertia and viscosity on the surface contact time in viscous media:

$$T_c = T_{c,H}\left(\frac{\rho_p + c_M\rho_f}{\rho_p}\right)^{2/5} \frac{1}{1 - 0.85St^{-1/10}}. \tag{3.24}$$

Here, $c_M \approx 0.73$ is the added-mass coefficient for a spherical body moving towards a wall in the moment of direct contact with the wall, and $T_{c,H}$ is the contact time

https://doi.org/10.1017/jfm.2012.343 Published online by Cambridge University Press

according to the theory of Hertz (3.19). Equation (3.24) extends the discussion of § 3.1 in the sense that the fluid entrained by the approaching particle alters the time of direct surface contact during the collision process. This phase hence in fact is not exactly equal to the same situation without fluid. For $St = 10$ the maximum of the ratio $T_c/T_{c,H} \approx 3$ is reached, decreasing for larger Stokes numbers. Nevertheless, in this situation we still use the term 'dry collision' for the phase of surface contact, as is customary in the literature, e.g. Joseph *et al.* (2001). Additional to the reasoning in § 2 above based on the required time step size for dry collision and fluid ($\Delta t_f \approx 63\Delta t_c$ in the example) we can now provide a refined argument based on physical grounds. The improved model for the collision time can be related to the particle relaxation time τ_r which characterizes the time necessary for the particle to adjust its velocity to an unsteady situation. Legendre *et al.* (2006) used the Schiller–Naumann formula for the drag (Schiller & Naumann 1933) to estimate the relaxation time by the expression

$$\tau_r = \frac{(\rho_p + c_M \rho_f) D_p^2}{18 \nu_f \rho_f (1 + 0.15 Re_p^{0.687})}. \tag{3.25}$$

A comparison of the contact time T_c and the relaxation time τ_r clearly shows that for typical cases T_c is several orders of magnitude smaller than τ_r. The situation can be illustrated by the collision of a glass sphere of density $\rho_p = 2500$ kg m^{-3} and diameter $D_p = 1.5$ mm in water at its terminal sedimentation velocity $u_\infty = 0.21$ m s^{-1} ($St = 89$, $Re_p = 320$). The contact time computed from (3.19) and (3.24) is $T_c = 1.81 \times 10^{-5}$ s, while the relaxation time according to (3.25) is $\tau_r = 4.51 \times 10^{-2}$ s. This corresponds to a ratio of $\tau_r/T_c \approx 2503$. For the example discussed in § 2 a ratio of $\tau_r/T_c \approx 2112$ is obtained. Hence, the problem of the strongly different time scales for particle motion without collision and surface contact persists over the entire range of collisions involving rebound in viscous media, with τ_r/T_c increasing for decreasing Stokes number.

The time step in a simulation can of course be reduced to $\Delta t \approx T_c/10$. But the large values of τ_r/T_c in the examples above suggest that, apart from being very costly, this is unnecessary, just leading to over-resolving the fluid motion in time. Alternatively, one could use sub-cycling to only advance the particle deformation in time during contact. The substantial scale separation between the characteristic times, however, calls for modelling the fast scales on one hand, and is the reason for its success on the other hand. In the following, the same global time step is used for the fluid equations as well as for the particle motion.

3.3.4. *Lubrication force*

To derive an analytical model for collisions in viscous fluids, Davis *et al.* (1986) and Barnocky & Davis (1988) assumed that the lubrication force dominates the motion of the sphere near a wall as it reduces speed during approach and rebound. This contribution can be quantitatively described by the lubrication theory of Brenner (1961) and Cox & Brenner (1967) who derived the relation

$$F_{n,pq}^{lub} = -\frac{6\pi \nu_f \rho_f g_{n,pq}}{\zeta_{n,pq}} \left(\frac{R_p R_q}{R_p + R_q} \right)^2. \tag{3.26}$$

The hydrodynamic forces begin to decelerate the particle at a certain distance from the wall, denoted $\zeta_{n,0}$, with the velocity of the particle at this point being $u_{in,0}$. Due to the action of the viscous forces the velocity of the particle is reduced to $u_{in} < u_{in,0}$ when it gets into direct contact with the wall. This distance is denoted $\zeta_{n,c}$ here, and

https://doi.org/10.1017/jfm.2012.343 Published online by Cambridge University Press

one would expect $\zeta_{n,c} = 0$. There are, however, two reasons to set $\zeta_{n,c} > 0$. The first is that all surfaces possess roughness, even if only very small. The second reason is that the description of the phenomena by means of Stokes flow (3.26) yields singular behaviour for $\zeta_{n,c} = 0$. Setting $\zeta_{n,c} > 0$ hence is a means to cope with both issues. In the subsequent phase of direct surface contact Barnocky & Davis (1988) used (3.21) as an expression for the rebound velocity at the end of the dry interface contact. Joseph (2003) later extended the analysis of Barnocky & Davis (1988) to the post-collision motion of the sphere by applying lubrication theory again to find the rebound velocity $u_{out,0}$ as the particle returns to its initial position $\zeta_{n,0}$. The resulting overall restitution coefficient e obtained with this simple model compares fairly well with the experimental measurements. This underpins the decomposition of the collision process into the three phases as described above: approach, surface contact (or 'dry collision') and rebound.

3.4. *Discussion of existing collision models*

3.4.1. *Motivation*

In the literature on discrete-element methods applied to collision-dominated flows widely used models are available such as the HSM and the SSM (Crowe *et al.* 1998). An easy-to-use model in viscous flows is also available in the form of the repulsive potential (RPM). These models constitute the state of the art so that comparison of any new model with these is desired. To make the paper self-contained they are next briefly recalled with the notation introduced above.

3.4.2. *Hard-sphere model*

The HSM according to Foerster *et al.* (1994) is based on an integrated form of the Newtonian equations of motion for the particle. The particle collisions are not resolved in time. Instead, the particle translational and rotational velocity after collision are determined by the integrated conservation law. As a consequence, the model is restricted to the contact of two particles at a time and the collision time is infinitesimally small.

The linear momentum balance and the angular momentum balance for particle p and q read

$$m_p(\boldsymbol{u}_{p,out} - \boldsymbol{u}_{p,in}) = \boldsymbol{F}, \tag{3.27}$$

$$m_q(\boldsymbol{u}_{q,out} - \boldsymbol{u}_{q,in}) = -\boldsymbol{F}, \tag{3.28}$$

and

$$I_p\left(\boldsymbol{\omega}_{p,out} - \boldsymbol{\omega}_{p,in}\right) = R_p \boldsymbol{n}_{pq} \times \boldsymbol{F}, \tag{3.29}$$

$$I_q(\boldsymbol{\omega}_{q,out} - \boldsymbol{\omega}_{q,in}) = R_q \boldsymbol{n}_{pq} \times (-\boldsymbol{F}), \tag{3.30}$$

respectively, with $\boldsymbol{F}$ being the force exerted on the particle p. Application to the collision of two particles p and q yields the collision rule for the normal velocity

$$(\boldsymbol{g}_{n,pq} \cdot \boldsymbol{n}_{pq})_{out} = -e\,(\boldsymbol{g}_{n,pq} \cdot \boldsymbol{n}_{pq})_{in} \tag{3.31}$$

and for the tangential velocity

$$(\boldsymbol{g}^{cp}_{t,pq} \times \boldsymbol{n}_{pq})_{out} = -\beta\,(\boldsymbol{g}^{cp}_{t,pq} \times \boldsymbol{n}_{pq})_{in}\,. \tag{3.32}$$

Here, β is the tangential restitution coefficient defined in (4.10) below, with $-1 \leqslant \beta \leqslant 1$, and $\beta = -1$ representing a perfectly smooth surface and $\beta = 1$ a perfectly rough surface.

https://doi.org/10.1017/jfm.2012.343 Published online by Cambridge University Press

3.4.3. *Soft-sphere model*

The SSM (Cundall & Strack 1979; Schwarzer 1995; Xu & Yu 1997) is based on the differential form of the Newtonian equations of motion of the particles. The collisions are fully resolved in time so that this model can be applied to multiple simultaneous particle collisions. Momentum and displacement of the particles are obtained for arbitrary times by solving the differential equations for normal and tangential motion. The macroscopic force describing the collision process is usually derived from a physically motivated microscopic approach. One of the most common expressions for the normal force is the one according to Hertz (3.15) combined with a damping force proportional to the relative normal velocity, as used by Stevens & Hrenya (2005) and Kruggel-Emden *et al.* (2007), for example. The SSM usually requires an excessive time step reduction in the case of an interface-resolving IBM or the use of reduced material stiffness compared to the experimental values as employed by Feng *et al.* (2010), for example. This is due to the different time scales for the fluid and the dry collision process addressed above.

3.4.4. *Repulsive potential*

In viscous fluids, the repulsive potential model (RPM) proposed by Glowinski *et al.* (1999) is often employed. This type of model is not based on strict physical reasoning but rather just attempts to prevent solid bodies from overlapping by a repulsive force in the normal direction. The expression of this force is

$$\boldsymbol{F}_{n,pq}^{col} = \frac{1}{\epsilon}(\boldsymbol{x}_p - \boldsymbol{x}_q)\,(\max\{0, -(\zeta_{n,pq} - \mathscr{S})\})^2, \tag{3.33}$$

where ϵ is a model constant depending on the problem considered and $\mathscr{S}$ the range of the repulsive force. Usually, $\mathscr{S} = 2h$ is chosen with h being the step size of the Eulerian grid. The model was successfully employed for the simulation of dilute suspensions, for example by Uhlmann (2008) in the case of a particle-laden flow in a vertical channel with $\epsilon = 8 \times 10^{-4} D_p/(\rho_f u_\infty^2)$. In other flow configurations, different prefactors are needed or may be advantageous (Glowinski *et al.* 2001; Pan & Glowinski 2002; Apte, Martin & Patankar 2009). With this model, material damping is neglected and hence the coefficient of restitution is equal to 1. Furthermore, ϵ is chosen *a priori*. High stiffness parameters potentially violate the stability criterion for time integration, while low stiffness yields an unphysically long collision process or in the limit may even allow a particle to run entirely through a physically solid wall as experienced in our early simulations. Another definition of the repulsive force was used by Wan & Turek (2006). Their model allows slight overlapping of surfaces and can handle more complex particle shapes provided an accurate calculation of the surface distance is performed. Effects of lubrication and material damping are not accounted for, however.

3.5. *Adaptive collision time model*

3.5.1. *Idea and structure of the model*

To avoid the problems mentioned above, a new approach is proposed here for the phase of direct surface contact, i.e. the phase of dry collision. The collision force normal to the surfaces is modelled by a spring force and a damping term, which accounts for the material damping. For the repulsive force the expression provided by the contact theory of Hertz (3.15) is used. The value of the coefficient k_n, however, is determined by an entirely different procedure as detailed below. The damping term is proportional to the normal surface velocity $\mathrm{d}\zeta_n/\mathrm{d}t = g_{n,pq}$ between the particles p and q.

https://doi.org/10.1017/jfm.2012.343 Published online by Cambridge University Press

The collision force then is given by

$$\boldsymbol{F}_{n,pq}^{col} = (k_n \zeta_n^{3/2} + d_n g_{n,pq}) \boldsymbol{n}_{pq}, \tag{3.34}$$

where d_n is the damping coefficient. As a result, the following nonlinear ordinary differential equation of second-order is obtained to model the dry collision process:

$$m_p \frac{\mathrm{d}^2 \zeta_n}{\mathrm{d}t^2} + d_n \frac{\mathrm{d}\zeta_n}{\mathrm{d}t} + k_n \zeta_n^{3/2} = 0. \tag{3.35}$$

As described in § 3.4.3 above, the time integration of the spring–mass–damper system (3.35) usually requires time steps Δt_c that are orders of magnitude lower than the corresponding maximum time step Δt_f of the fluid-solver if physically realistic values of the parameters corresponding to the employed pairing of materials are used. Therefore, it is proposed here to stretch the collision in time such that it takes approximately $T_c = 10\Delta t_f$ thus avoiding the extremely expensive reduction of Δt_f to match Δt_c. The idea is to determine the stiffness and damping in this equation using an optimization procedure in order to achieve the desired rebound velocity u_{out} and collision time T_c by requiring the solution of (3.35) to fulfil

$$\zeta_n(T_c) = 0, \tag{3.36}$$

$$g_{n,pq}(T_c) = u_{out}. \tag{3.37}$$

The rebound velocity u_{out} is given by (3.21) with experimental data being used for e_{dry}. This procedure is applied for each individual collision. Since the coefficients are adapted in each collision to fit the requirements, the model is termed adaptive collision time model (ACTM). The computation of the unknown coefficients d_n and k_n can be done at low cost by an iterative procedure described in appendix A. The value of $T_c/\Delta t_f = 10$ could in principle be modified if desired, but this is not recommended to avoid problems similar to the ones observed with the HSM, as discussed below.

It is important to observe that in the limiting case in which Δt_f is reduced to $\Delta t_{c,H}$ the exact microscopic trajectory of Hertzian collision is recovered, i.e. the model automatically switches itself off. Observe also that the ACTM can be implemented with any discretization scheme in space for the fluid, like adaptive unstructured grids, immersed boundary, etc. and with any discretization scheme in time.

3.5.2. *Determining initial values on physical grounds*

Appropriate initial values are often crucial for the performance of iterative schemes. Here, physical arguments are employed for their determination. Since damping is low in most cases, $d_n = 0$ is used as initial guess in all simulations presented here. With different materials, choosing a somewhat larger value might slightly improve the behaviour, though.

Good initial values for the stiffness are found from the collision time given by the contact theory of Hertz according to (3.19). For particle–wall collisions where particle and wall are of the same material, (3.19) reduces to

$$T_c = 3.218 \left(\frac{m_p}{k_n} \right)^{2/5} u_{in}^{-1/5}. \tag{3.38}$$

Hence, for a given collision time T_c the initial stiffness is obtained from

$$k_n = 18.578 \frac{m_p}{\sqrt{T_c^5 u_{in}}}. \tag{3.39}$$

https://doi.org/10.1017/jfm.2012.343 Published online by Cambridge University Press

An analogous approximation is used for particle–particle collisions. If the particles are of equal size and of the same material, the collision time according to (3.19) is

$$T_c = 2.439\left(\frac{m_p}{k_n}\right)^{2/5} u_{in}^{-1/5} \tag{3.40}$$

so that a good initial value for the stiffness is

$$k_n = 9.289\frac{m_p}{\sqrt{T_c^5 u_{in}}}. \tag{3.41}$$

Generalizations for other pairings can be derived analogously if required.

3.5.3. *Limiter for low Stokes numbers*

In many simulations the global time step is kept nearly constant. Hence, the desired collision time in the ACTM is also nearly constant. In such a case, the normal stiffness has to be increased if the impact velocity of the particle decreases, (3.39) and (3.41). For Stokes numbers below the critical value no rebound of the colliding particles is expected, so that the concept of a finite, stretched collision is inapplicable.

Therefore, if the Stokes number is below a critical value, a limiter for the normal stiffness is introduced. The stiffness then is computed from (3.38), now with u_{in} replaced by

$$u_{in,crit} = St_{in,crit}\frac{9}{2}\frac{\rho_f}{\rho_p}\frac{\nu_f}{R_p}$$

where St_{crit} is the critical Stokes number (note that St_{in} is the value at $\zeta_n = \zeta_{n,c}$, different from St defined in (3.23) which is taken at $\zeta_n = \zeta_{n,0}$). A value of $St_{crit} = 1$ is used in all cases here. Material damping during the dry contact is not accounted for in this case. In the limiting case the stiffness provided by the contact theory of Hertz (1882) is reached, hence the small scales are resolved without additional modelling.

3.5.4. *Performance of the ACTM*

In a first step, numerical experiments were conducted to determine the number of time steps over which to stretch the collision. Some of these are displayed figure 3 for two Stokes numbers, $St = 27$ and $St = 152$. In fact, two counteracting mechanisms can be observed. If the number of time steps is too small the model resembles the HSM where the rebound of the particle is too fast for the surrounding fluid to follow with the given temporal resolution, so that excessive reduction of the rebound height is observed (figure 1). If on the other hand the stretching in time is large physical realism is lost as well and leads to slightly increased rebound heights (dash-dotted curves in figure 3). The reported data show that stretching over 10 time steps provides good results avoiding both undesirable limits. The better agreement for larger Stokes number is intended as these collisions involve higher kinetic energy.

Quantitative data on the performance of the ACTM for typical configurations is presented in table 1. The computation time required for the ACTM is very small in comparison to the total time of the fluid solver per time step. The latter heavily depends on domain size, particle loading, etc., and can hence not be quantified in general here. An order of magnitude can however be provided by a typical production run. For a configuration with 10^8 Eulerian grid points and 500 freely moving particles resolved with $D_p/h \approx 20$ the cost of the ACTM was 6.4×10^{-3} % of the total CPU time.

https://doi.org/10.1017/jfm.2012.343 Published online by Cambridge University Press

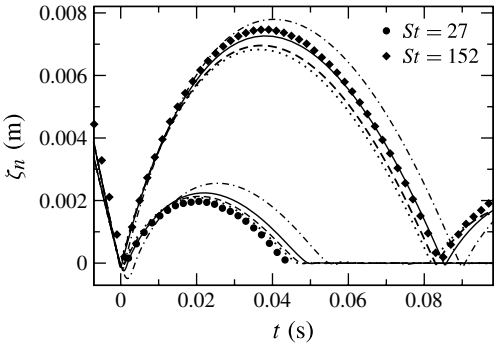


FIGURE 3. Normal impact of spheres on a glass wall with $St = 27$ and $St = 152$. Surface distance ζ_n versus time. The dry collision is resolved with: $\cdots\cdots$, 5; $- - -$, 7; ——-, 10 and $\cdot - \cdot - \cdot$, 20 time steps. Symbols: experiment of Gondret *et al.* (2002).

Material	R_p (m)	ρ_p (kg m^{-3})	u_{in} (m s^{-1})	St	e_{dry}	T_c (s)	m	t_{ACTM} (s)
Steel	2.5×10^{-3}	7800	0.870	742	0.97	1.656×10^{-4}	4	7×10^{-3}
Steel	1.5×10^{-3}	7800	0.873	2413	0.97	9.821×10^{-5}	4	7×10^{-3}
Steel	1.5×10^{-3}	7800	0.873	2413	0.6	9.821×10^{-5}	7	10×10^{-3}
Teflon	3.0×10^{-3}	2150	1.03	79 000	0.8	1.682×10^{-4}	7	9×10^{-3}
Teflon	3.0×10^{-3}	2150	2.06	158 000	0.8	8.410×10^{-5}	7	11×10^{-3}
Teflon	3.0×10^{-3}	2150	2.06	158 000	0.6	8.410×10^{-5}	11	17×10^{-3}

TABLE 1. Determination of k_n and d_n with the ACTM. Number of iterations m and wall-clock time t_{ACTM} for the iterative procedure in a single time step with one collision. Steel and Teflon spheres of radius R_p bouncing on a glass wall are considered. The cases with $e_{dry} = 0.6$ are artificial, though, to show that for low values of this parameter the method does not degrade. In all cases the resolution of the particle is $D/h \approx 20$ and the desired collision time is $T_c = 10\Delta t_f$. The computations were performed on an SGI Altix 4700.

3.5.5. *Lubrication model*

When the gap between the surfaces of the collision partners is small and their relative velocity is non-negligible, fluid is squeezed out of the gap upon approach and pushed back into the gap upon rebound. Viscous forces hence become important in these phases of approach and rebound and can lead to sizeable dissipation. The ACTM thus needs to be supplemented by an appropriate kind of 'subgrid-scale model' accounting for the film between the surfaces at times when it is too thin to be resolved by the Eulerian grid. The model amounts to determining a so-called lubrication force which is always directed opposite to the relative velocity and hence dissipative.

The approach is similar to the one of Ladd (1997) who proposed calculating the missing part of the hydrodynamic force using analytic expressions. An explicit expression for drag on a particle of radius R_p approaching another particle of radius R_q steadily with velocity $g_{n,pq}$ was given by Brenner (1961) and Cox & Brenner (1967) and was also used by other authors (Nguyen & Ladd 2002; Ten Cate *et al.* 2002; Apostolou & Hrymak 2008). The lubrication model for particle–particle interactions

https://doi.org/10.1017/jfm.2012.343 Published online by Cambridge University Press

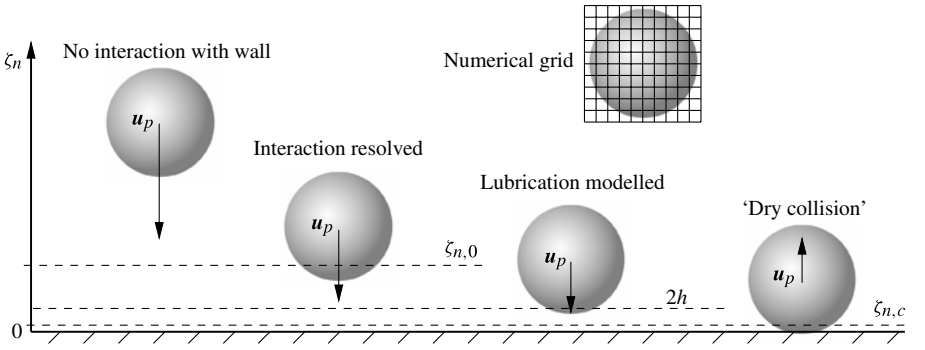


FIGURE 4. Summary of the present approach in the form of a sketch illustrating the resolved and the modelled contributions during the different phases of a wall-normal collision of a particle with a wall. The horizontal axis corresponds to the time.

used here is based on (3.26) and reads

$$\boldsymbol{F}_{n,pq}^{lub} = \begin{cases} 0, & 2h < \zeta_{n,pq} \\ -\dfrac{6\pi\nu_f\rho_f g_{n,pq}}{\zeta_{n,pq}}\left(\dfrac{R_pR_q}{R_p+R_q}\right)^2\boldsymbol{n}_{pq}, & \zeta_{min}^{lub} \leqslant \zeta_{n,pq} \leqslant 2h \\ 0, & \zeta_{n,pq} < \zeta_{min}^{lub}. \end{cases} \tag{3.42}$$

A cut-off distance ζ_{min}^{lub} is used to prevent the lubrication force from reaching its singularity at zero normal distance, where ζ_{min}^{lub} corresponds to the natural surface roughness, hence

$$\zeta_{min}^{lub} = \zeta_{n,c}. \tag{3.43}$$

For particle–wall interactions, with $R_q \to \infty$, (3.42) reduces to

$$\boldsymbol{F}_{n,w}^{lub} = \begin{cases} 0, & 2h < \zeta_{n,w} \\ -\dfrac{6\pi\nu_f\rho_f g_{n,w}}{\zeta_{n,w}}R_p^2\boldsymbol{n}_w, & \zeta_{min}^{lub} \leqslant \zeta_{n,w} \leqslant 2h \\ 0, & \zeta_{n,w} < \zeta_{min}^{lub}. \end{cases} \tag{3.44}$$

The functional principle of the lubrication model is sketched in figure 4. For surface distances $\zeta_n > \zeta_{n,0}$ the particle motion is resolved by the IBM and no influence of the wall is felt (see § 3.3.2 for more information about the definition of $\zeta_{n,0}$). If the particle approaches closer and the surface distance is in the range $\zeta_{n,0} > \zeta_n > 2h$, the particle motion still is resolved and no modelling of the particle–wall interaction is required. The particle then is more and more decelerated by the increasing pressure in the gap between particle and wall. Only if the surface distance becomes smaller than $\zeta_n < 2h$ does the lubrication model set in until dry surface contact at $\zeta_n = \zeta_{n,c}$.

From a technical point of view, the dry collision process (3.35) is slightly modified by replacing ζ_n with $\zeta_n - \zeta_{n,c}$ such that the collision force sets in at $\zeta_n = \zeta_{n,c}$ instead of $\zeta_n = 0$. Note that $\zeta_{n,c}$ is very small. In the situations below, $\zeta_{n,c} \approx 10^{-4}D_p$ and $2h \approx 10^{-1}D_p$ so that $h/\zeta_{n,c} \approx 500$. The importance is that, whatever grid is used, features larger than $2h$ can be resolved and need not be modelled. Equations (3.42) and (3.44) hence can also be applied for excessively refined grids.

https://doi.org/10.1017/jfm.2012.343 Published online by Cambridge University Press

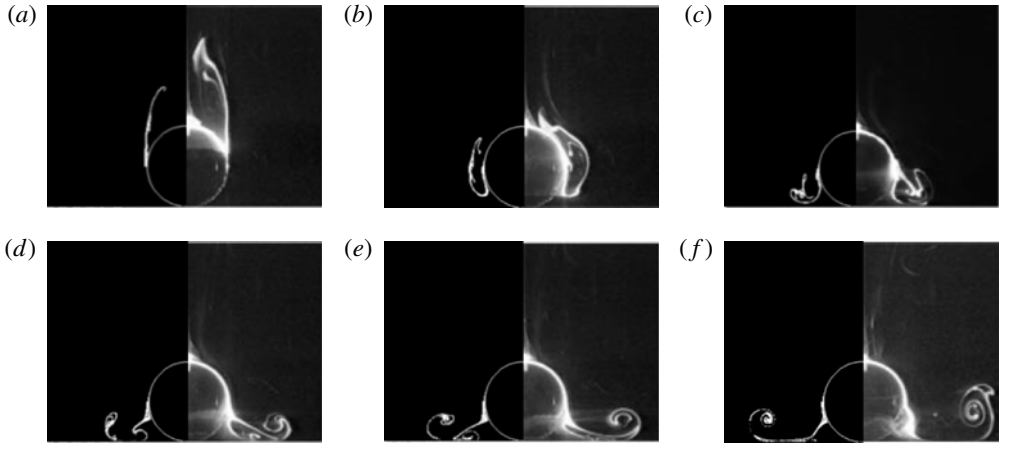


FIGURE 5. Numerical and experimental determination of the flow around a sphere impacting on a wall. The left-hand halves of the images were obtained with the present simulation method while the right-hand halves contain the experimental data of Eames & Dalziel (2000). The times are (*a*) $t^* = 0$ (at this instant the sphere reaches the wall), (*b*) $t^* = 1$, (*c*) $t^* = 2$, (*d*) $t^* = 3$, (*e*) $t^* = 4$, (*f*) $t^* = 8$, with $t^* = tu_p/D_p$ (simulation and experiment started well before $t^* = 0$).

3.6. *Validation*

3.6.1. *Normal particle–wall collisions without rebound, approach phase*

First, a case is investigated where no rebound occurs. A sphere is moved towards the wall with constant speed and is stopped when it touches the surface. The flow patterns for this problem were investigated numerically and experimentally by Leweke *et al.* (2004, 2006) and Thompson *et al.* (2007), as well as experimentally by Eames & Dalziel (2000). The experiment of Eames & Dalziel (2000) is used here for reference. This was also done in the numerical works of Ardekani & Rangel (2008) and Vanella & Balaras (2009).

In the present simulation the computational domain is $\Omega = [0; L_x] \times [0; L_y] \times [0; L_z]$ with $L_x = L_y = L_z = 40$ mm, discretized with $N_x \times N_y \times N_z = 256 \times 256 \times 256$ points. The spatial resolution of the sphere is $D_p/h \approx 50$ where h is the cell size of the equidistant Cartesian grid, and the surface of the sphere discretized with $N_L = 7855$ marker points. The Reynolds number before the impact is $Re_p = 850$ and the Stokes number is $St = 295$. Since in the experiment the sphere was stopped by the apparatus when it touched the wall, the coefficient of restitution is $e = 0$ in this case. This is in contrast to a freely moving sphere, where at this Stokes number a significant rebound occurs.

Figure 5 shows visualizations of the simulated flow using passive tracer particles which can be compared directly with the experiment of Eames & Dalziel (2000) where dye was used to track vortex structures. When the sphere approaches the wall, a recirculation zone is seen in its wake (figure 5*a*). After the impact, a system of vortex rings develops from the initially trailing separated region at the rear (figure 5*b*). It passes the sphere (figure 5*c*) and impacts on the wall (figure 5*d,e*) where it is finally convected outwards (figure 5*f*). The figure shows that the approach phase is very well matched by the simulation and illustrates the usefulness of the present method for the detailed study of particle–fluid interactions with collisions.

https://doi.org/10.1017/jfm.2012.343 Published online by Cambridge University Press

Case	Material	D_p (m)	ρ_p (kg m^{-3})	ρ_f (kg m^{-3})	ν_f (s m^{-2})	St	Re_p	e_{dry}
1	Steel	3×10^{-3}	7800	965	1.0363×10^{-4}	6	6	0.97
2	Steel	6×10^{-3}	7800	965	1.0363×10^{-4}	27	30	0.97
3	Steel	3×10^{-3}	7800	953	2.0986×10^{-5}	60	66	0.97
4	Steel	4×10^{-3}	7800	953	2.0986×10^{-5}	100	110	0.97
5	Steel	3×10^{-3}	7800	935	1.0695×10^{-5}	152	165	0.97
6	Steel	6×10^{-3}	7800	953	2.0986×10^{-5}	193	212	0.97
7	Steel	5×10^{-3}	7800	920	5.4348×10^{-6}	742	788	0.97
8	Steel	3×10^{-3}	7800	998	1.0040×10^{-6}	2413	2785	0.97
9	Teflon	6×10^{-3}	2150	1.2	1.5417×10^{-5}	79 000	400	0.80

TABLE 2. Physical parameters of particles and fluids used in experiments and the present simulations of spherical particles impacting on a glass wall. The surface roughness of the steel and Teflon spheres is $\zeta_{n,c} = 3\times10^{-7}$ m and $\zeta_{n,c} = 9\times10^{-7}$ m, respectively.

3.6.2. *Normal particle–wall collisions with rebound*

Now, the ACTM is applied to various configurations with rebound, comparing the results with the experimental data of Gondret *et al.* (2002). The computational domain $\Omega = [0; L_x]\times[0; L_y]\times[0; L_z]$ with $L_x = L_y = L_z = 13.3D_p$ was discretized with $N_x\times N_y\times N_z = 256\times256\times256$ points. A time step corresponding to $CFL = 0.6$ was used in all cases. The spatial resolution of the sphere is $D_p/h \approx 20$. The surface of the sphere is represented by $N_L = 1159$ marker points. The dry coefficient of restitution e_{dry} was taken as a material parameter from the experiment. Its value and those of the other physical parameters are reported in table 2. Table 3 shows a comparison of the collision time T_c with the values from the theory of Hertz and the maximum surface penetration $-\zeta_n^{min}$ compared to the Hertz theory. Data are provided for the collision of a sphere with radius $D_p = 3$ mm onto a glass wall at various Stokes numbers corresponding to cases 1, 3, 5, and 8 of table 2.

The comparison of $T_c/T_{c,H}$ shows that the problem of different time scales for fluid solver and collision is more pressing for small Stokes numbers. This can be explained by the following theoretical consideration. According to (3.19) the collision time reduces with increasing impact velocity according to $T_{c,H}\propto u_{in}^{-1/5}$. A typical fluid time scale is $\tau_f = R_p/u_{in}$. For fixed resolution of the particle, $D_p/h = \text{const.}$, hence the time step of the fluid solver is $\Delta t_f \propto \tau_f$. For an adequate resolution of the collision $T_c \propto \Delta t_f$ is required, so that $T_c \propto u_{in}^{-1}$ which yields the relation

$$\frac{T_c}{T_{c,H}} \propto u_{in}^{-4/5}. \tag{3.45}$$

The ratio $T_c/T_{c,H}$ hence decreases with increasing impact velocity u_{in}. This also confirms the result in § 3.3.3 where the separation of time scales was discussed in terms of relaxation time τ_r and $T_{c,H}$.

Table 3 shows that the price to pay for stretching the collision process in time is an increase in surface penetration compared to the exact value. The same occurs with lowering the stiffness of the SSM in an *ad hoc* manner, without this being quantified in most cases.

Let us now address the impact of stretching the collision on the flow field in the vicinity of the particle. Figure 6 shows plots of the vector field together with contour plots of the wall-normal velocity at the end of an unstretched and of a stretched collision with $St = 152$. Both flow fields are extremely similar so that the

https://doi.org/10.1017/jfm.2012.343 Published online by Cambridge University Press

https://doi.org/10.1017/jfm.2012.343 Published online by Cambridge University Press

Case	u_∞ (m s^{-1})	k_n	T_c (s)	$T_{c,H}$ (s)	$T_c/T_{c,H}$	$-\zeta_n^{min}/D_p$	$-\zeta_{n,H}^{min}/D_p$	$\zeta_n^{min}/\zeta_{n,H}^{min}$
1	0.217	5245	3.71×10^{-3}	1.95×10^{-5}	191	9.12×10^{-2}	4.77×10^{-4}	191
1	0.217	2 063 104	3.39×10^{-4}	1.95×10^{-5}	18	8.36×10^{-3}	4.77×10^{-4}	18
3	0.459	34 514	1.50×10^{-3}	1.67×10^{-5}	90	7.82×10^{-2}	8.69×10^{-4}	90
5	0.583	84 842	1.02×10^{-3}	1.59×10^{-5}	63	6.60×10^{-2}	2.05×10^{-3}	63
8	0.925	999 264	3.39×10^{-4}	1.54×10^{-5}	24	3.56×10^{-2}	1.52×10^{-3}	24

TABLE 3. Simulation of the collision of spherical particles with diameter $D_p = 3$ mm and a glass wall in various fluids. The spatial resolution of the sphere is $D_p/h \approx 20$. Reported is the collision time T_c used in the simulations, the collision time $T_{c,H}$ according to the theory of Hertz (3.19), the maximum surface overlapping $-\zeta_n^{min}/D_p$ of the ACTM and the maximum surface overlapping $-\zeta_{n,H}^{min}/D_p$ according to Hertz (3.20). The stiffness from (3.16) is $k_n = 2.648 \times 10^9$ N m^{-1}. To avoid overcrowding only the most significant cases of table 2 are included here.

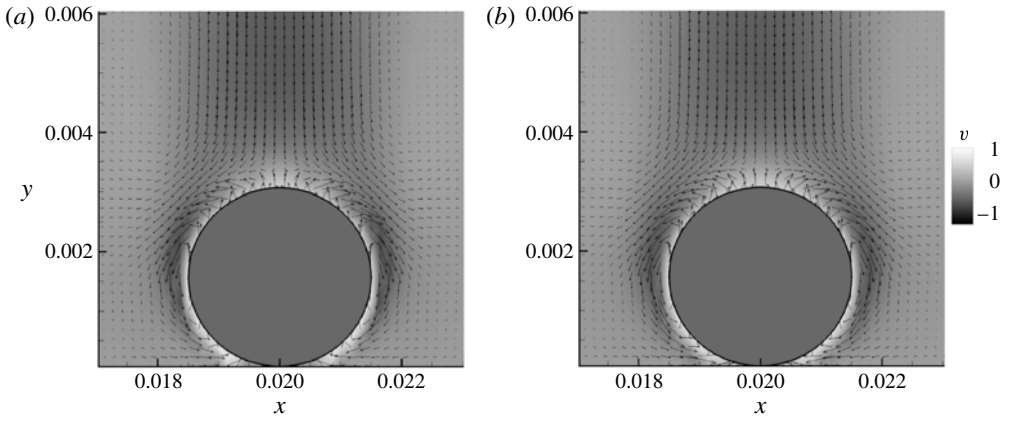


FIGURE 6. Comparison of the flow field at the end of the unstretched and stretched collisions. Parameters according to case 5 of table 2. (*a*) Vector field of the centreplane, with grey-scale according to the vertical component, obtained for the unstretched collision computed according to the theory of Hertz. (*b*) The same data from a simulation with a stretched collision computed with the ACTM at the end of the stretched collision process. The plots show only part of the domain.

flow structure around the particle is practically the same. Furthermore, the correct loss of the kinetic energy of the particle is ensured during the collision since stiffness and damping are adjusted with ACTM.

The advantage of the present model in this respect is two-fold. First, the stretching in time, i.e. the weakening of the interaction and hence the inter-penetration, is limited to the absolute minimum required for conducting the simulation with the chosen time step. Second, the user can decide beforehand by estimating the Stokes number in the computed flow and conducting simple tests whether a certain amount of surface penetration is deemed acceptable or not. In the latter case the time step Δt_f can be reduced in a very controlled way.

In figure 7(*a*) the particle trajectories are displayed for cases 2, 4, 5, 7 of table 2 and figure 7(*b*) shows the overall restitution coefficient e. Comparison with the experimental data of Gondret *et al.* (2002) demonstrates the extremely good match of the model with the experiment.

The coefficient e was computed in a post-processing step. For each individual collision, the velocity $u_{in,0}$ was found from the velocity-versus-time plot. It was taken to be the value just before the particle starts to decelerate due to the influence of the wall at a certain distance $\zeta_{n,0}$ and was determined by visual inspection. The velocity $u_{out,0}$ then is the value obtained when the particle rebounds and reaches the same distance from the wall. This was done for each collision individually since the distance $\zeta_{n,0}$ varies with the Stokes number. Note, that the restitution coefficient is evaluated here only to compare the results with experimental data. The simulation itself only employs e_{dry}. The excellent agreement of the particle trajectories also indicates that the same amount of energy is dissipated in the experiment and the simulation.

In figure 7(*a*), the second curve from above displaying multiple collisions is for $St = 152$ which is the value before the first collision. Due to viscous dissipation and material damping kinetic energy is lost and subsequent rebounds have lower and lower

https://doi.org/10.1017/jfm.2012.343 Published online by Cambridge University Press

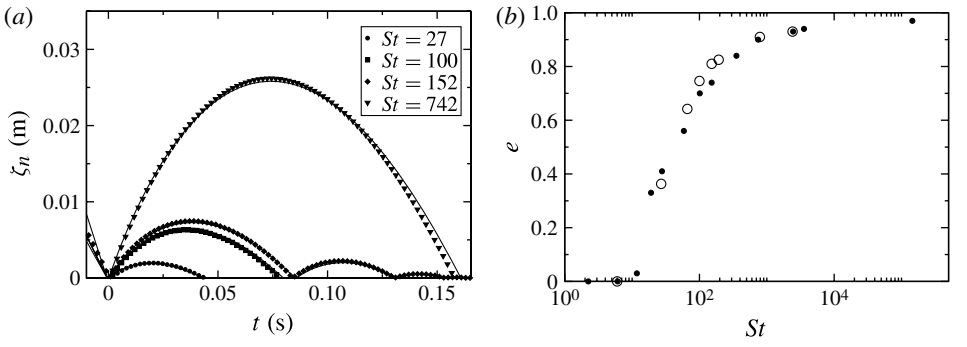


FIGURE 7. Collisions of steel spheres with a glass wall. (*a*) Particle position versus time for various Stokes numbers. Symbols, experiment by Gondret *et al.* (2002); ——-, present results with ACTM. (*b*) Normal coefficient of restitution for different Stokes numbers. ○, Present simulations with the parameters provided in table 2, cases 1–8; ●, experimental data of Gondret *et al.* (2002).

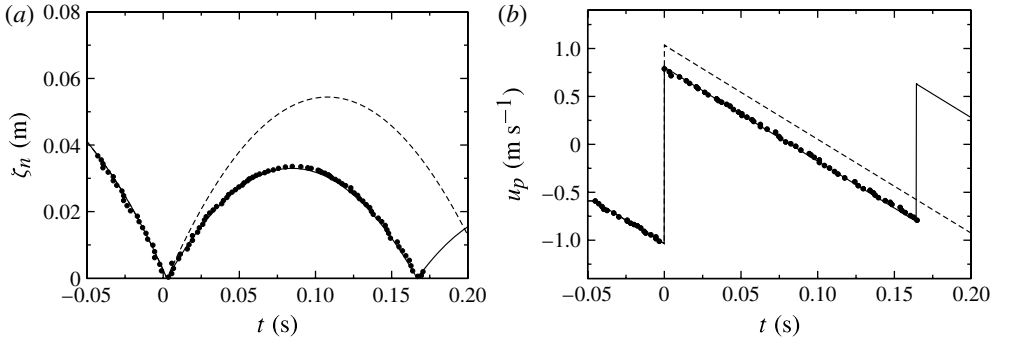


FIGURE 8. Normal impact of a Teflon bead on a glass wall in air. The coefficient of restitution is $e_{dry} = 0.8$. (*a*) Particle position versus time, (*b*) particle velocity versus time. ●, Experiment Gondret *et al.* (2002); ——-, ACTM with $e_{dry} = 0.8$; − − −, ACTM without material damping, i.e. $e_{dry} = 1$.

height. The Stokes number of these collision reduces to 78, 39 and 21, respectively. Nevertheless, they are represented very accurately, which illustrates the capability of the model to adopt to each individual collision due to optimization of coefficients in each case.

Case 9 in figure 8 designates an experiment where a Teflon bead impacts on a glass wall with air as ambient fluid. A significant amount of kinetic energy is dissipated during the phase of direct contact yielding a dry coefficient of restitution equal to $e_{dry} = 0.8$. The ACTM predicts the trajectory very accurately since the appropriate damping is determined by the optimization procedure described in § 3.5 above. In figure 8 the particle position and the velocity are displayed over time. For comparison a simulation with $e_{dry} = 1$ was performed as well. These data show again the excellent agreement obtained with the present model.

https://doi.org/10.1017/jfm.2012.343 Published online by Cambridge University Press

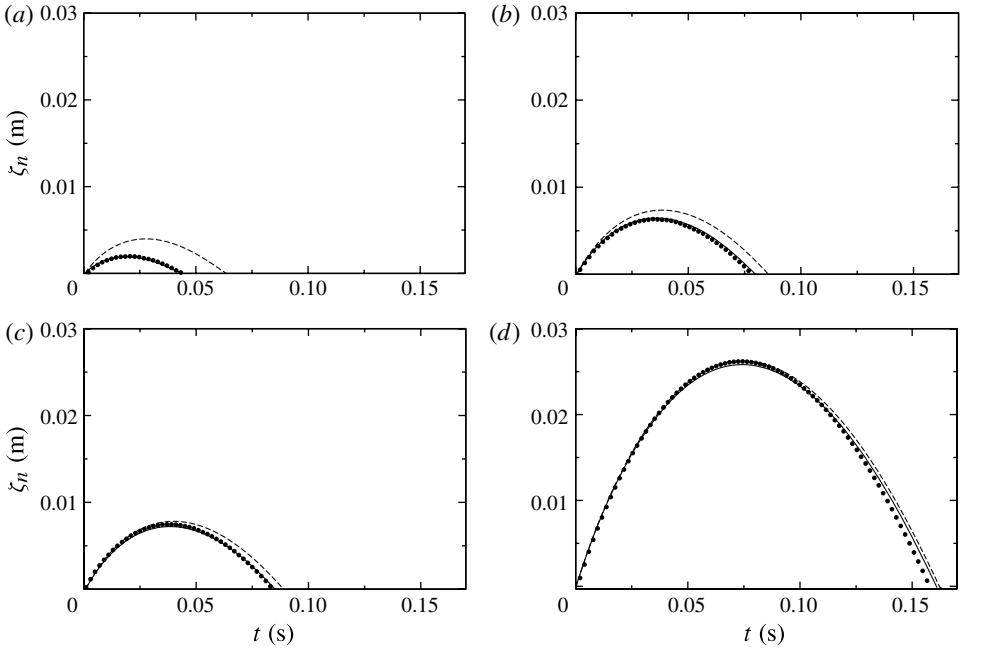


FIGURE 9. Normal particle–wall collisions with ACTM for Cases 2, 4, 5, 7 of table 2. ——-, Present simulation with lubrication model (3.42); – – –, simulation without lubrication model; •, experiment of Gondret *et al.* (2002). (*a*) $St = 27$, $Re_p = 30$; (*b*) $St = 100$, $Re_p = 110$; (*c*) $St = 152$, $Re_p = 165$; (*d*) $St = 742$, $Re_p = 788$.

3.6.3. *Performance of the lubrication model*

Figure 9 addresses the relevance of the lubrication model by displaying the trajectories employing the present approach with and without the lubrication model (3.44). The data for the full model are those of figure 7(*a*). It is apparent that at lower Stokes numbers the particle is significantly decelerated due to the viscous forces. Hence, the lubrication model becomes more and more important for the accurate prediction of the rebound trajectory of the particle when the Stokes number is reduced. At $St = 27$ the rebound height is doubled when the lubrication model is omitted, for example.

3.6.4. *Normal collisions of two particles*

Detailed experiments on particle–particle collisions immersed in a viscous fluid were performed by Yang & Hunt (2006) using a pendulum string. In their experimental findings for purely normal collisions, e depends on the Stokes number in a similar way as observed for particle–wall collisions. This is supported by figure 10(*a*) displaying the results of Joseph *et al.* (2001) and Gondret *et al.* (2002) for particle–wall collisions together with the data of Yang & Hunt (2006). The numerical simulations reported here were performed with the same configurations as described in table 2 (cases 1–8). Instead of the lower plane wall, a particle with the same radius as the approaching particle was placed fixed in the flow field. A freely moving particle approaching the stationary particle at its terminal sedimentation velocity was introduced in such a way that collisions are purely normal, i.e. the vector of relative velocity and the vector between the centres of mass are collinear. In all cases the ACTM was used.

https://doi.org/10.1017/jfm.2012.343 Published online by Cambridge University Press

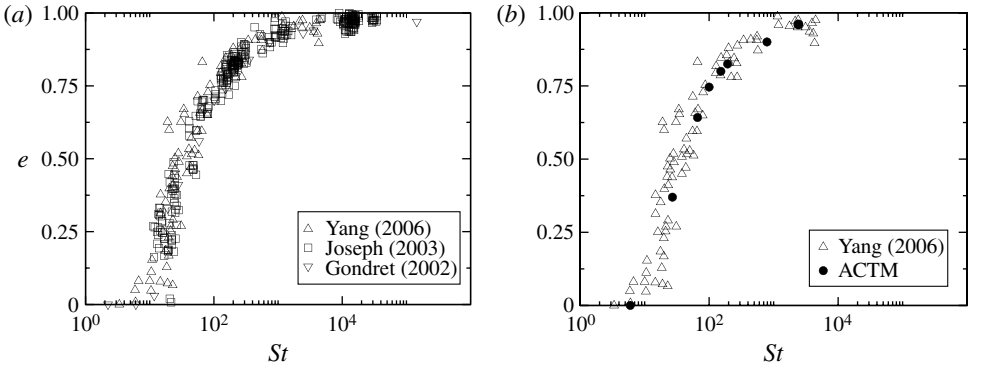


FIGURE 10. Coefficient of restitution e for normal particle–particle and particle–wall collisions. (a) Experiments with particle–particle collisions (Yang & Hunt 2006) compared to the experimental data for particle–wall collisions of Gondret *et al.* (2002) and Joseph *et al.* (2001). (b) Particle–particle collisions simulated with the present model in comparison with the experimental data of Yang & Hunt (2006).

The numerical results for particle–particle collisions and the experimental data of Yang & Hunt (2006) are shown in figure 10(b). These results confirm the excellent performance of the ACTM for particle–particle collisions also.

4. Modelling of oblique collisions

4.1. *Introduction*

In usual particle-laden flows oblique particle–wall and particle–particle collisions occur, where in contrast to purely normal collisions described in § 3, the collision partners also have a tangential interaction. In this section a numerical model for such collisions in interface-resolving simulation of spherical particles in viscous fluid is presented. The basic idea is to decompose an oblique collision into a normal and a tangential component and to employ a separate collision model in each direction. This is supported by data from the literature (Joseph & Hunt 2004; Yang & Hunt 2006). We start by first describing the experimental and numerical findings for oblique dry collisions. Subsequently, the experimental results for oblique particle–wall and particle–particle collisions in viscous fluids are reported. Based on these data numerical models are proposed.

4.2. *Dry oblique collisions*

For normal particle–wall and particle–particle collisions the theory of Hertz provides an adequate description of the dry collision (Stevens & Hrenya 2005). For the oblique contact of two elastic spheres pressed together at constant normal load Mindlin (1949) developed a contact model which later was extended to more complex normal loading by Mindlin & Deresiewicz (1953). Maw, Barber & Fawcett (1976, 1977) performed numerical simulations based on these contact models. For dry collisions the latter authors found that the trajectory of a sphere colliding with a wall only depends on two non-dimensional parameters as follows. The first parameter is the modified radius of gyration

$$\chi = \frac{(1-\nu)(1+K^{-2})}{2-\nu} \tag{4.1}$$

https://doi.org/10.1017/jfm.2012.343 Published online by Cambridge University Press

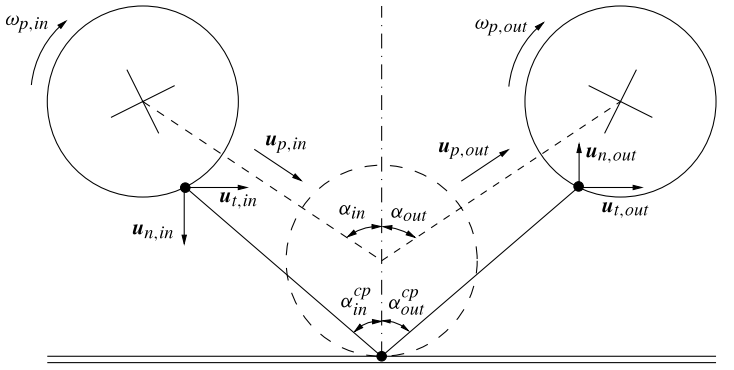


FIGURE 11. Sketch of the oblique collision of a spherical particle with a wall. Observe that both states 'in' and 'out' according to (4.4), (4.5) and (4.6) involve vanishing distance from the wall. Such a distance is drawn here for clear visibility only.

with ν the Poisson ratio. In (4.1),

$$K^2 = \frac{\int r^2 \rho_p \, \mathrm{d}V}{R_p^2 \int \rho_p \, \mathrm{d}V} \tag{4.2}$$

is the non-dimensional radius of gyration, with ρ_p being the density of the particle which in this equation is allowed to vary inside the particle. Equation (4.2) yields $K^2 = 2/5$ for a homogeneous sphere. The second parameter is the normalized local angle of contact for impact and rebound

$$\psi_{in} = \frac{2(1-\nu)u_{t,in}}{\mu(2-\nu)u_{n,in}}, \quad \psi_{out} = \frac{2(1-\nu)u_{t,out}}{\mu(2-\nu)u_{n,in}}. \tag{4.3}$$

Here, $\mu = F_t/F_n$ is the coefficient of sliding friction, with F_n the normal and F_t the tangential force. The quantities $u_{t,in}$ and $u_{t,out}$ are the instantaneous values of the tangential surface velocity at the contact point immediately before and after contact. The tangential impact velocity is defined as

$$u_{t,in} = g_{t,pq}^{cp} \quad (\zeta_n = 0, t = 0) \tag{4.4}$$

and the tangential rebound velocity as

$$u_{t,out} = g_{t,pq}^{cp} \quad (\zeta_n = 0, t = T_c), \tag{4.5}$$

where T_c is the time interval during which the surfaces are in direct contact. Note that normalization in (4.3) is performed with the impact velocity

$$u_{n,in} = g_{n,pq}^{cp} \quad (\zeta_n = 0, t = 0) \tag{4.6}$$

for both quantities, ψ_{in} and ψ_{out}. Figure 11 displays the situation of an oblique collision of a sphere colliding with a flat wall and illustrates the notation.

According to Maw *et al.* (1976, 1977), the normalized local angle of incidence ψ_{in} and the radius of gyration χ determine whether or not the impact commences in gross slip. In figure 12 the numerical results of Maw *et al.* (1976, 1977) for the normalized local angle of rebound versus the normalized local angle of incidence are displayed for a material with $\nu = 0.3$ and $\chi = 1.4412$. Numerical results were obtained by those

https://doi.org/10.1017/jfm.2012.343 Published online by Cambridge University Press

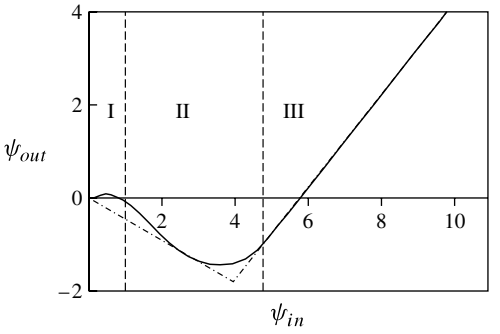


FIGURE 12. Normalized local angle of rebound ψ_{out} versus angle of incidence ψ_{in}. Numerical result of Maw *et al.* (1976) for a homogeneous solid sphere with $\nu = 0.3$ and $\chi = 1.4412$ (data extracted from the reference). Roman numerals indicate the regimes described in the text with I: $0 < \psi_{in} \leqslant 1$, II: $1 < \psi_{in} \leqslant 4.764$, III: $4.764 < \psi_{in}$. Dash-dotted lines show the approximation of Walton & Braun (1986) discussed in the text.

authors for a wide range of values of ψ_{in} and χ and may be qualitatively described as follows. For small angles of incidence, $\psi_{in} \leqslant 1$, the normal load F_n is larger than the tangential force F_t and the surfaces stick during contact. This corresponds to regime I in figure 12. In this regime micro-slip may occur caused by tangential elastic recovery when the midpoint of the impact in time is passed and the contact area shrinks. In the intermediate range of incidence angles, $1 < \psi_{in} \leqslant (4\chi - 1)$, the collision starts with substantial slip but the sliding velocity drops to zero before the end of the collision (regime II). The negative rebound angles observed are caused by the tangential compliance of the surfaces like in a nonlinear spring–mass system. For $(4\chi - 1) < \psi_{in}$ (regime III) the collision occurs entirely in gross slip and the tangential force is at all times given by μ multiplied with the normal force. More recently, Kharaz, Gorham & Salman (1999, 2001) experimentally investigated the collision of spheres with a flat surface, while Lorenz, Tuozzolo & Louge (1997) studied the impact of spherical particles made of various materials colliding with similar beads rigidly affixed to a plate. All these experiments fully confirmed the prediction of Maw *et al.* (1976, 1977).

As noted by Joseph & Hunt (2004), a drawback of the otherwise general description of Maw *et al.* (1976, 1977) is that in order to evaluate ψ from experimental measurements, a prior quantitative evaluation of the friction coefficient μ is required. To this end the angles α_{in}^{cp} and α_{out}^{cp} as defined in figure 11 are used to define a local angle of incidence Ψ_{in} and a local angle of rebound Ψ_{out} according to

$$\frac{u_{t,in}}{u_{n,in}} = \tan(\alpha_{in}^{cp}) \equiv \Psi_{in}, \tag{4.7}$$

$$\frac{u_{t,out}}{u_{n,out}} = \frac{u_{t,out}}{e_{dry} u_{n,in}} = \tan(\alpha_{out}^{cp}) \equiv \frac{1}{e_{dry}} \Psi_{out}. \tag{4.8}$$

The graph of Ψ_{out} versus Ψ_{in} can then be obtained from measurements of u_t and u_n and be used to distinguish between the three regimes as described above. According to Foerster *et al.* (1994) the sliding regime (III) allows extraction of the value of μ from

$$\mu = \frac{\Psi_{in} - \Psi_{out}}{(1 + e_{dry})(1 + 1/K^2)}. \tag{4.9}$$

https://doi.org/10.1017/jfm.2012.343 Published online by Cambridge University Press

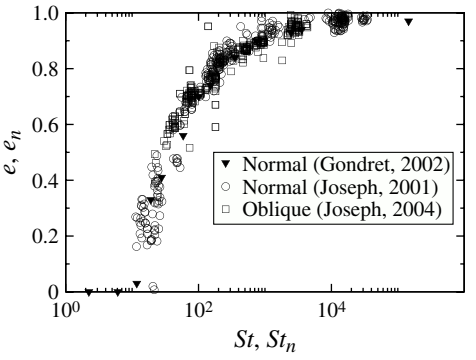


FIGURE 13. Effective coefficient of restitution e_n versus normal Stokes number St_n for the normal component in an oblique collision compared to the same date in a purely normal collision, $e = f(St)$.

Based on the theory of Maw *et al.* (1976, 1977), Walton & Braun (1986) and Walton (1993) presented a simplified macroscopic model for oblique collisions (dash-dotted line in figure 12) characterizing them by three parameters: (*a*) the normal coefficient of restitution e_{dry}; (*b*) the tangential coefficient of restitution (Lun & Savage 1987)

$$\beta = -\frac{u_{t,out}}{u_{t,in}} = -\frac{\Psi_{out}}{\Psi_{in}}, \tag{4.10}$$

for non-sliding collisions; and (*c*) the coefficient of friction μ for sliding collisions.

4.3. *Oblique collisions in viscous fluids*

The theoretical results of Maw *et al.* (1976, 1977) and the experimental data of Kharaz *et al.* (1999, 2001) discussed in the previous sections are valid for dry collisions, i.e. for negligible viscosity of the interstitial fluid. In the following we turn to oblique collisions in viscous fluids.

The experiments of Joseph & Hunt (2004) and Yang & Hunt (2006) support the decomposition of such an oblique collision into its normal and tangential components. The normal component of the particle motion hence is described by the corresponding coefficient of restitution based on the wall-normal component of the velocity

$$e_n = -\frac{u_{n,out,0}}{u_{n,in,0}}, \tag{4.11}$$

similar to (3.22) and the Stokes number St_n computed with $u_{n,in,0}$. Figure 13 shows that the experimental correlation for e_n versus St_n in the oblique case follows the particle–wall collision results of Joseph *et al.* (2001) and Gondret *et al.* (2002) for perpendicular incidence. The observed scatter is due to the high sensitivity of the process to experimental conditions.

For the tangential component of the collision, Joseph & Hunt (2004) discovered a similar dependence of the local angles of impact and rebound, Ψ_{in} and Ψ_{out}, to that observed in dry systems. In figure 14(*a*) the experimental results for glass and steel spheres of various diameters in various fluids are shown. By computing the normalized local angle of contact according to (4.3) the individual plots of the local angles of impact and rebound in figure 14(*a*) collapse onto a single curve as shown

https://doi.org/10.1017/jfm.2012.343 Published online by Cambridge University Press

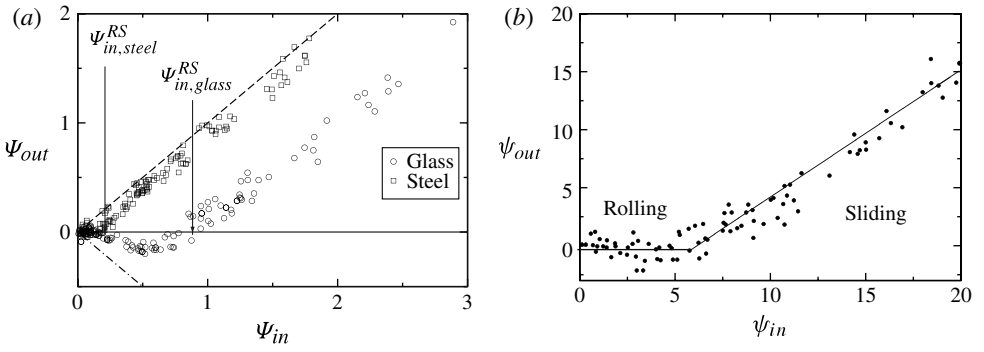


FIGURE 14. Oblique collision of glass spheres and steel spheres of various diameters with a wall in various fluids. (*a*) Local rebound angle Ψ_{out} (4.8) versus local impact angle Ψ_{in} (4.7). The lines indicate three types of collisions with $\mu = 0$: ——-, $\beta = 0$; $-\ -\ -$, $\beta = 1$; $\cdot - \cdot - \cdot$, $\beta = -1$. (*b*) Normalized local rebound angle ψ_{out} versus normalized local impact angle ψ_{in} (4.3) for the collisions shown in (*a*). Experimental data provided by G. Joseph(2009, personal communication).

in figure 14(*b*), similar to figure 12 for dry oblique collision. (Note the difference between capital Ψ and lower-case ψ in figure 14.)

To evaluate (4.3), the coefficient of sliding friction μ is required. For collisions in viscous fluids the value of μ can change dramatically compared to dry collisions (Joseph & Hunt 2004; Yang & Hunt 2006). Due to the interstitial fluid, μ is generally lower than the dry coefficient of friction. For rough surfaces the measured value of μ is comparable to dry systems (Joseph 2003; Joseph & Hunt 2004) since the surface asperities interact piercing through the lubrication layer. An analytical approach for the computation of the friction coefficient for immersed oblique collisions was presented by Joseph & Hunt (2004) taking into account the pressure and temperature dependence of the viscosity.

4.4. *Idea and modelling strategy*

The experimental findings assembled above support the possibility of decomposing an oblique collision into a normal and a tangential part. Hence it seems convenient to employ such an approach for modelling oblique collisions in a simulation. The normal part of the collision process is modelled using the ACTM described in § 3.5 while the tangential contribution is treated separately from the normal contribution. Note, however, that since the latter is stretched in time, the tangential part taking place simultaneously is stretched in time by the same amount.

Since Mindlin (1949) and Mindlin & Deresiewicz (1953) performed the first theoretical analysis of the oblique impact of spheres, numerous proposals for modelling the tangential forces have been presented, e.g. by Vu-Quoc *et al.* (2004) and Kruggel-Emden *et al.* (2008). Nevertheless, the underlying physics of the tangential forces in an oblique collision are not yet fully understood. Therefore a modelling approach based on experimental findings is proposed here for this part.

4.5. *Modelling the tangential part*

4.5.1. *Existing models and basic concept*

In the experimental work of Joseph & Hunt (2004) the effective angles of impact Ψ_{in} and rebound Ψ_{out} were measured for various materials in various fluids.

https://doi.org/10.1017/jfm.2012.343 Published online by Cambridge University Press

In figure 14(*b*) two main regimes of particle motion may be identified. If the effective angle of impact Ψ_{in} is lower than a critical value Ψ_{in}^{RS}, the relative surface velocity at the contact point is zero and the particle performs purely rolling motion. If Ψ_{in} is larger than Ψ_{in}^{RS}, the particle performs purely sliding motion.

Based on this observation a model for tangential collisions is proposed here which contains two experimental parameters depending on material data and surface properties alone. The first parameter is the critical value for the effective angle of impact Ψ_{in}^{RS} separating the regimes of sliding and rolling motion. The second parameter is the coefficient of sliding friction μ.

The model is realized as follows: at the beginning of the collision, Ψ_{in} is computed and compared to Ψ_{in}^{RS}. If $\Psi_{in} > \Psi_{in}^{RS}$ sliding motion is assumed and the collision force in the tangential direction is given by the well-known Coulomb friction law

$$\boldsymbol{F}_t^{col} = -\mu |\boldsymbol{F}_n| \boldsymbol{t}, \tag{4.12}$$

where $\boldsymbol{t}$ is a shorthand for $\boldsymbol{t}_{pq}^{cp}$ defined by (3.9). If $\Psi_{in} < \Psi_{in}^{RS}$, the particle is assumed to roll and hence the relative surface velocity at the contact point has to be zero.

In the present paper, two models for the tangential force from the literature are considered for reference, both developed in the context of the DEM. The first is the approach of Haff & Werner (1986), where the tangential force is assumed to be proportional to the relative surface velocity in the tangential direction:

$$\boldsymbol{F}_t^{col} = -d_t |\boldsymbol{g}_t^{cp}| \boldsymbol{t}. \tag{4.13}$$

The second approach is the one of Cundall & Strack (1979), where the tangential force is modelled as a spring acting in the direction tangential to the contact plane:

$$\boldsymbol{F}_t^{col} = -k_t \boldsymbol{\zeta}_t. \tag{4.14}$$

The elongation of the spring in the tangential direction $\boldsymbol{\zeta}_t$ is defined as

$$\boldsymbol{\zeta}_t(t) = \int_0^{T_c} \boldsymbol{g}_{t,pq}^{cp} \, \mathrm{d}t. \tag{4.15}$$

Modifications of this model for use with ACTM are presented in appendix B.

In DEM simulations, the model of Haff & Werner (1986) yields reliable results for systems where the particles collide during finite time but do not rest statically as for example in the case of a sand heap (Pöschel & Schwager 2005). In the model of Cundall & Strack (1979) the tangential displacement $\boldsymbol{\zeta}_t$ is dependent on the collision history.

With both models, (4.13) and (4.14), the constants d_t and k_t have to be determined *a priori* with a substantial drawback: if in (4.13) the tangential damping d_t is chosen too low, the slip of the surfaces may become too large and no rolling motion is imposed. If d_t is too large the simulation may become unstable due to the unphysical large rotational acceleration of the particle at the begin of the contact. The same problems are observed with the second model according to (4.14).

4.5.2. *The adaptive tangential force model*

To alleviate the deficiencies of the existing models described above, a new parameter-free model is proposed here. It ensures slip-free rolling motion and can be applied to particle–wall and particle–particle collisions. The model is first described for the more complex case of particle–particle collisions, then for particle–wall collisions.

https://doi.org/10.1017/jfm.2012.343 Published online by Cambridge University Press

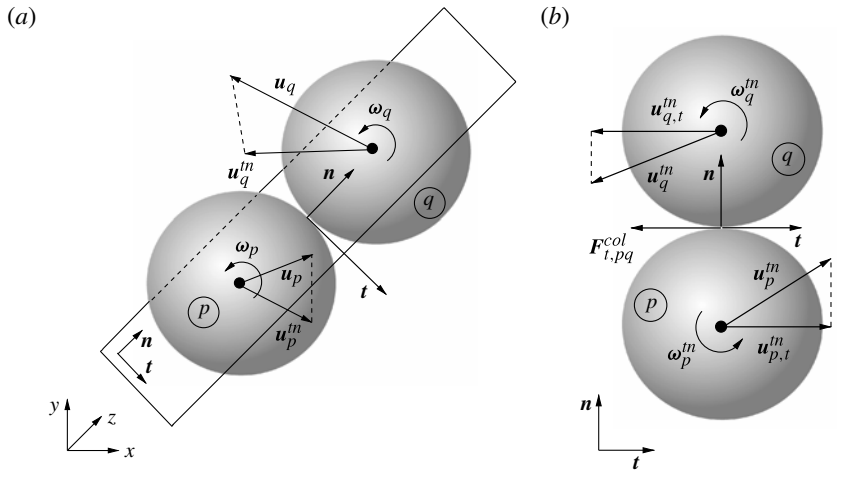


FIGURE 15. Oblique collision of two spherical particles. (*a*) Plane defined by the vector normal and tangential to the contact point in a three-dimensional view. (*b*) Velocity vectors in the $\boldsymbol{t}$–$\boldsymbol{n}$ plane, view perpendicular to the plane. (Note that $\boldsymbol{\omega}_p$ and $\boldsymbol{\omega}_q$ in (*a*) are vectors, while ω_p^{tn} and ω_q^{tn} in (*b*) are scalars.)

With rolling motion of two particles p and q the relative surface velocity at the contact point is $\boldsymbol{g}_t^{cp}$ vanishing at each instant in time during contact. The new model is now based on the idea that a tangential contact force is determined exactly in such a way that $\boldsymbol{g}_t^{cp} = 0$. This is imposed in time-discrete form and described here for an explicit Euler scheme with the upper index i referring to the time step. The present implementation actually employs a Runge–Kutta method so that in (4.16) and (4.17) below, the time step Δt is to be replaced by $2\alpha_k \Delta t$ where α_k is the Runge–Kutta coefficient of the kth sub-step and the upper index i replaced with the index k for the Runge–Kutta sub-step.

To compute the required tangential collision force $\boldsymbol{F}_t^{col}$ consider the discrete linear momentum equation for particle p, which is in contact with particle q:

$$\boldsymbol{u}_p^{i+1} = \boldsymbol{u}_p^i + \Delta t \frac{\boldsymbol{F}_{t,pq}^{col}}{m_p}, \tag{4.16}$$

and the equation for angular momentum

$$\boldsymbol{\omega}_p^{i+1} = \boldsymbol{\omega}_p^i + \Delta t \frac{\boldsymbol{M}_p^{col}}{I_p}. \tag{4.17}$$

The particle motion in the laboratory system is sketched in figure 15(*a*) for the case when $\boldsymbol{\omega}_p$ is parallel to $\boldsymbol{\omega}_q$ for ease of presentation, but (3.1), (3.9) and the following equations hold for arbitrary orientation of $\boldsymbol{\omega}_p$ and $\boldsymbol{\omega}_q$. Now, consider the particle motion in a plane defined by the normal vector $\boldsymbol{n} = \boldsymbol{n}_{pq}$ according to (3.1) and the tangential vector $\boldsymbol{t} = \boldsymbol{t}_{pq}^{cp}$ according to (3.9) as sketched in figure 15(*b*). The relative tangential surface velocity $g_{t,pq}^{cp}$ at time $t + \Delta t$, given by (3.10), (4.16) and (4.17), is

$$g_{t,pq}^{cp} = \frac{2\Delta t F_{t,pq}^{col}(I_p + m_p R_p^2)}{I_p m_p} + u_{p,t}^{tn} - u_{q,t}^{tn} - R_p(\omega_p^{tn} + \omega_q^{tn}), \tag{4.18}$$

https://doi.org/10.1017/jfm.2012.343 Published online by Cambridge University Press

where

$$u_{p,t}^{tn} = \boldsymbol{u}_p \cdot \boldsymbol{t} \tag{4.19}$$

is the particle velocity tangential to the contact point and

$$\omega_p^{tn} = \boldsymbol{\omega}_p \cdot (\boldsymbol{n} \times \boldsymbol{t}) \tag{4.20}$$

the angular velocity in the $\boldsymbol{t}$–$\boldsymbol{n}$ plane. The tangential force $F_{t,pq}^{col}$ which has to be applied for a vanishing relative tangential surface velocity

$$g_{t,pq}^{cp} \stackrel{!}{=} 0 \tag{4.21}$$

then is

$$F_{t,pq}^{col} = \frac{I_p m_p (u_{q,t}^{tn} - u_{p,t}^{tn} + R_p(\omega_p^{tn} + \omega_q^{tn}))}{2\Delta t (I_p + m_p R_p^2)}. \tag{4.22}$$

Transforming $F_{t,pq}^{col}$ back into the laboratory system yields the force $\boldsymbol{F}_{t,pq}^{col} = F_{t,pq}^{col}\boldsymbol{t}$ exerted on particle p. The tangential collision force on the companion particle q is given by $\boldsymbol{F}_{t,qp}^{col} = -\boldsymbol{F}_{t,pq}^{col}$. The restriction to a collision force in a purely tangential direction is directly realized here by geometrical constraints. For particle–wall collisions or collisions with a fixed particle the tangential collision force is found from

$$F_{t,pw}^{col} = \frac{I_p m_p (-u_{p,t}^{tn} + R_p \omega_p^{tn})}{\Delta t (I_p + m_p R_p^2)}. \tag{4.23}$$

An alternative way of computing the tangential collision force directly in the laboratory system without transformation to the $\boldsymbol{t}$–$\boldsymbol{n}$ plane is presented in appendix C.

With the present model no momentum is transferred during direct contact from one particle to the other by the components $\boldsymbol{\omega}_p \cdot \boldsymbol{n}$ and $\boldsymbol{\omega}_q \cdot \boldsymbol{n}$. Since the force $\boldsymbol{F}_{t,pq}^{col}$ is determined in a way adapted to the time step, to the collision parameters as well as to the requirement (4.21), this model is called *adaptive tangential force model* (ATFM). It consists of (4.12) stretched in time if $\Psi_{in} > \Psi_{in}^{RS}$ and (4.22), (4.23) for $\Psi_{in} > \Psi_{in}^{RS}$.

4.5.3. *Performance of the ATFM*

In the following, the stability and the performance of the two existing contact models for granular media (4.13), (4.14) and the new model (4.22) is addressed with the ACTM of § 3.5 applied for the normal contribution. For this validation exercise a sphere rolling on an inclined wall in a fluid-filled container is considered and the relative slip of the surfaces is computed for various values of the model parameters in (4.13) and (4.14). The surface slip s of spherical particles can be expressed as

$$s = \frac{\|\boldsymbol{u}_p\| - R_p\|\boldsymbol{\omega}_p\|}{\|\boldsymbol{u}_p\|}. \tag{4.24}$$

The computational domain $\Omega = [0; L_x] \times [0; L_y] \times [0; L_z]$ with $L_x = L_y = L_z = 13.3D_p$ contains $N_x \times N_y \times N_z = 256 \times 256 \times 256$ grid points. A time step corresponding to $CFL = 0.6$ was used in all cases. The spatial resolution of the sphere is $D_p/h \approx 20$ and the surface of the sphere was discretized with $N_L = 1159$ marker points. The wall is inclined by an angle of $\alpha = 30°$. The particle density is $\rho_p = 7780$ kg m^{-3}, gravity $g = 9.81$ m s^{-2} and the fluid is water with $\rho_f = 998$ kg m^{-3} and $\nu_f = 1.004 \times 10^{-6}$ m^2 s^{-1}. A sketch of the configuration is shown in figure 16(*a*).

https://doi.org/10.1017/jfm.2012.343 Published online by Cambridge University Press

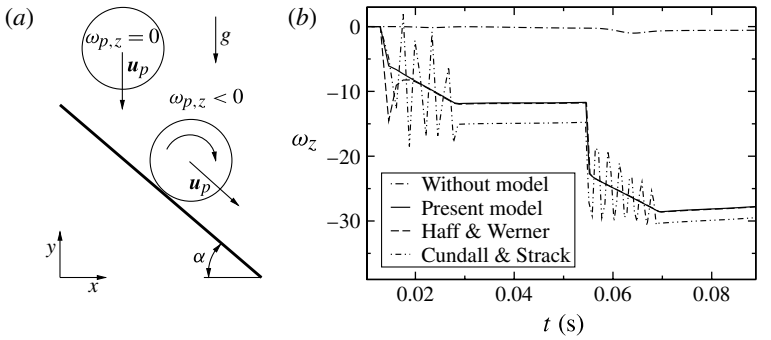


FIGURE 16. Particle in water falling onto an inclined wall. (*a*) Sketch of the configuration. (*b*) Angular velocity for various collision models. The data for the model of Haff & Werner were obtained with $d_t = 1\ \mathrm{N\ s\ m^{-1}}$ and those for the model of Cundall & Strack with $k_t = 1\ \mathrm{N\ m^{-1}}$. The label 'without model' refers to the ACTM for the normal component and the absence of a model for the tangential component.

Haff & Werner (4.13)		Cundall & Strack (4.14)		ATFM (4.22)
d_t (N s m^{-1})	s	k_t (N m^{-1})	s	s
0.1	2.4×10^{-2}	0.1	2.9×10^{-3}	1.1×10^{-3}
0.5	5.2×10^{-3}	0.5	1.3×10^{-3}	
1.0	2.6×10^{-3}	1.0	1.0×10^{-4}	
5.0	Unstable	5.0	Unstable	

TABLE 4. Relative surface slip of a particle rolling on an inclined wall using various collision models. The ATFM does not require any parameter to be specified.

The model constants d_t in (4.13) and k_t in (4.14) are required to be small enough to ensure a stable time integration for the equations of motion of the particles, so that their choice is always a compromise between exact imposition of no-slip between the particles, i.e. rolling motion, and numerical stability. The maximum relative slip observed during the simulation is provided in table 4 for various model parameters.

The numerical results for the angular velocity of the particle are shown in figure 16(*b*). Without tangential force being introduced by a corresponding model no rotation of the particle is generated and it just slides along the wall. The models (4.13) and (4.14) tend to exhibit oscillations with the set of parameters used in the computations. The model of Haff & Werner yields a substantial undershoot at the beginning with good performance subsequently. The model of Cundall & Strack exhibits non-tolerable oscillations. For lower values of d_t (results not shown here), the model (4.13) yields a large relative slip. For the model (4.14), lowering k_t reduces the amplitude of the oscillations, but these cannot be fully removed. The newly developed ATFM (4.22) yields a very smooth behaviour of the angular velocity while the remaining surface slip of the particle is very small. Hence, a stable and accurate time integration is ensured without any additional calibration.

4.5.4. *Lubrication model in the tangential direction*

During the oblique approach of the particles, the hydrodynamic force has a normal component and a tangential component. The latter results in torque acting on the

https://doi.org/10.1017/jfm.2012.343 Published online by Cambridge University Press

ζ_n/R_p	10^{-1}	10^{-2}	10^{-3}	10^{-6}	10^{-8}
M_r^*/M_t^*	3.103	3.421	3.573	3.760	3.814

TABLE 5. Ratio of the non-dimensional torque M_r^* due to rotational motion of a sphere near a wall to the torque M_t^* induced by the translational motion of the sphere resulting from expressions (4.28) and (4.29).

particles. Goldman, Cox & Brenner (1967) presented an analysis of a spherical particle performing rotation near a plane wall and translation parallel to the wall, employing the Stokes solution for low Reynolds numbers. Due to the linearity of the equations of motion and considering absolute values (with $\boldsymbol{\omega}_p \cdot \boldsymbol{u}_p = 0$), the torque M on the particle is the sum of two separate effects: the torque from translational motion M_t^* and from rotational motion M_r^*, i.e.

$$M = 8\pi\nu_f\rho_f R_p^2(u_p M_t^* + \omega_p R_p M_r^*), \tag{4.25}$$

where

$$M_t^* = \frac{M_t}{8\pi\nu_f\rho_f u_p R_p^2} \tag{4.26}$$

is the non-dimensional torque due to translation and

$$M_r^* = \frac{M_r}{8\pi\nu_f\rho_f\omega_p R_p^3} \tag{4.27}$$

the non-dimensional torque due to rotation, respectively. The asymptotic limit yields the solution (Goldman *et al.* 1967)

$$M_t^* = -\frac{1}{10}\ln\left(\frac{\zeta_n}{R_p}\right) - 0.1895 \tag{4.28}$$

for a non-rotating sphere propagating parallel to a wall and

$$M_r^* = -\tfrac{2}{5}\ln\left(\frac{\zeta_n}{R_p}\right) - 0.3817 \tag{4.29}$$

for a sphere rotating about an axis parallel to a plane wall without translation. The ratio M_r^*/M_t^* resulting from these two expressions is reported in table 5 for various distances ζ_n/R_p. This ratio becomes even larger for smaller distances to the wall. As a consequence, Joseph (2003) argued that in an oblique collision where a sphere without spin approaches a wall no significant rotation is generated until contact with the wall since the counter-torque M_r^* by the beginning of rotation of the sphere is large enough to damp any translation-induced rotational motion M_t^*. The torque generated by the velocity component of the centre of mass tangential to the surface during an oblique approach or rebound does not set a non-rotating particle in rotation. On the same basis Joseph (2003) argued, for a spinning sphere approaching a wall, that any initial angular velocity decays slowly due to the dominating contribution of M_r^* in (4.25) for the total torque M.

With the present method the interface of the particle is resolved, hence the viscous forces are directly captured by the IBM. The situation is different, though, when

https://doi.org/10.1017/jfm.2012.343 Published online by Cambridge University Press

the particle is very close to the wall as particle rotation might be generated due to unresolved viscous forces in the narrow gap that is smaller than the grid size. Popov & Psakhie (2007) found from the Stokes flow approximation that the tangential forces in the gap between the approaching or rebounding surfaces generated by tangential motion are much smaller than those generated by the normal motion. For collision modelling in simulations of flow laden with point particles, Apostolou & Hrymak (2008) argued in a similar way that when the particles are in close proximity the dominating contribution to the lubrication force is the one due to the normal component so that only this component is considered in their work. For these reasons, no lubrication model is employed here in the tangential direction.

4.5.5. *Exchange of linear and angular momentum during stretched collisions*

In the ACTM, the collisions are stretched in time but the stiffness and damping in (3.34) are determined such that the coefficient of normal restitution e_{dry} is identical to that of a collision governed by the theory of Hertz. Therefore, the change of momentum in the normal direction is the same for both collision processes, i.e.

$$(u_{out} - u_{in})m_p = u_{in}(e_{dry} - 1)m_p = \int_{t_0}^{T_{c,H}} F_{n,H}^{col}\,\mathrm{d}t \stackrel{!}{=} \int_{t_0}^{T_c} F_n^{col}\,\mathrm{d}t, \tag{4.30}$$

where the subscript H denotes Hertzian contact.

For oblique collisions, depending on the critical local angle of incidence Ψ_{in}^{RS}, two regimes of tangential interaction can be distinguished. For $\Psi_{in} < \Psi_{in}^{RS}$, rolling motion is assumed and the tangential force is determined such that the relative surface velocity is zero (4.22). Hence, the angular velocities after the collision are identical for the stretched and the unstretched collision, i.e. $\Delta\omega_p = \Delta\omega_p^H$. Therefore, the exchange of angular momentum is identical in both cases. Only the angular orientation of the particles at the end of the contact is different since the duration of the collision is not the same. This is definitely tolerable.

In the case of sliding motion ($\Psi_{in} > \Psi_{in}^{RS}$) the tangential force is given by the Coulomb law (4.12). The change of angular momentum for an unstretched collision then is

$$\Delta\omega_p^H I_p = R_p\mu \int_{t_0}^{T_{c,H}} F_{n,H}^{col}\,\mathrm{d}t, \tag{4.31}$$

while the change of angular momentum for a stretched collision is

$$\Delta\omega_p I_p = R_p\mu \int_{t_0}^{T_c} F_n^{col}\,\mathrm{d}t. \tag{4.32}$$

Combining (4.30)–(4.32) yields $\Delta\omega_p = \Delta\omega_p^H$. Again, the angular momentum exchange is identical for the stretched and the unstretched collision. As in the case of rolling contact, the angular orientation of the particle is different in both cases. It is hence concluded that during a stretched collision neither additional linear momentum nor additional angular momentum is generated in comparison to an unstretched collision governed by the theory of Hertz.

4.6. *Validation for particle–wall collisions*

In this section we have supplemented the ACTM for normal collisions, enhanced by the lubrication model for normal collisions, with the ATFM for the tangential forces. The resulting combined model, ACTM plus lubrication model plus ATFM, is

https://doi.org/10.1017/jfm.2012.343 Published online by Cambridge University Press

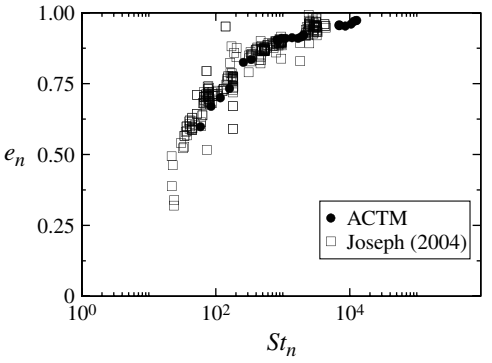


FIGURE 17. Coefficient of restitution e obtained in the present simulations with different angles of incidence compared to the experiment for a glass sphere impacting a plane wall at various angles of incidence by Joseph & Hunt (2004).

Fluid	ρ_f (kg m^{-3})	ν_f (m^2 s^{-1})	Particle	ρ_p (kg m^{-3})	e_{dry}	μ	Ψ_{in}^{RS}
Water	998.0	1.007×10^{-6}	Glass	2540	0.97	0.15	0.95
Glycerol 33%	1082.7	2.309×10^{-6}	Steel	7780	0.97	0.02	0.25
Glycerol 45%	1114.9	4.036×10^{-6}					

TABLE 6. Physical properties of the fluids and particles used in the experiment of Joseph & Hunt (2004) and in the present simulations.

termed *adaptive collision model* (ACM). This final combination is now validated for general oblique collisions using the experimental data of Joseph & Hunt (2004). The computational domain $L_x \times L_y \times L_z = [0; 0.1693\ \text{m}] \times [0; 0.1693\ \text{m}] \times [0; 0.1693\ \text{m}]$ was discretized with $N_x \times N_y \times N_z = 256 \times 256 \times 256$ equidistant points. A sphere with diameter $D_p = 12.7$ mm is considered which corresponds to a spatial resolution of $D_p/h = 19.2$. The surface of the sphere is covered with $N_L = 1159$ marker points, and the properties of the fluids and materials used in experiment and simulation are reported in table 6. The effective coefficient of sliding friction μ and the critical effective angle of impact Ψ_{in}^{RS} required for the collision model in the table were taken from the experimental data of Joseph & Hunt (2004).

For the normal part of the collision the ACTM described in § 3.5 was employed and for the tangential interaction the ATFM (4.22) was employed. The numerical results for the normal coefficient of restitution are displayed in figure 17 and correspond very well to the experimental data. Figure 18 displays results for the rebound angle with steel and glass particles in various fluids obtained with the present model, compared to experimental data for the same configuration. The performance of the model is very satisfactory and could hardly be better in the light of the measurement uncertainty. Only the slightly negative values of Ψ_{out} for Ψ_{in} around 0.5 are not captured in the case of glass spheres, i.e. a rough surface. This is expected by construction and certainly tolerable when suspensions are simulated. If needed, it might be accounted for by a slight modification of the model for tangential collisions using the tangential coefficient of restitution (4.10).

https://doi.org/10.1017/jfm.2012.343 Published online by Cambridge University Press

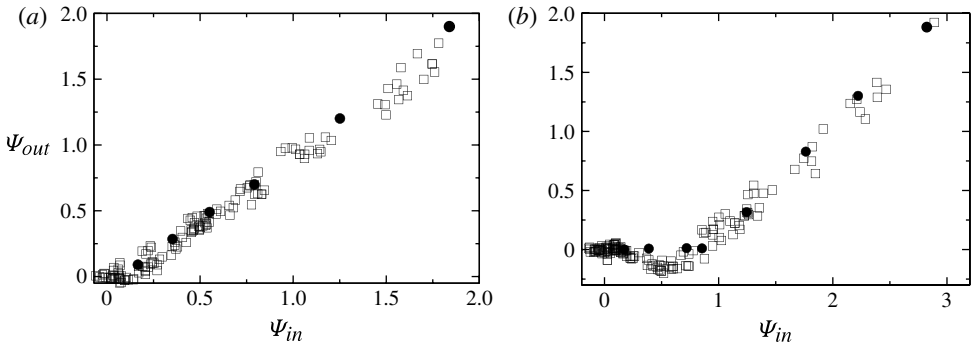


FIGURE 18. Local angle of rebound Ψ_{out} (4.8) versus local angle of impact Ψ_{in} (4.7). (*a*) Steel in various fluids, (*b*) glass in various fluids. □, Experiment of Joseph & Hunt (2004); •, present model.

5. Concluding remarks

The present paper provides efficient and accurate collision modelling for interface-resolving simulations of flows laden with spherical particles. In such flows not only normal but general oblique particle–particle and particle–wall collisions occur. First, various available collision models were applied to collisions in viscous fluids demonstrating their failure when employed with an existing continuous-forcing IBM, even in the case of a normal collision. A similar assessment was performed for tangential collisions in § 4.5.3.

Improvements on different levels were achieved, based on a detailed study of the available literature. First, the discretization method was enhanced to remove numerical effects dominating the physical models, which is reported in a companion paper (Kempe & Fröhlich 2012). A lubrication model was then introduced to account for fluid films between collision partners which are thinner than the cell size of the grid. A main achievement of the paper is the concept of a judiciously determined stretching of the collision process in time. This was implemented in the form of the adaptive collision time model (ACTM) designed to conserve physical realism to the largest possible extent. The model was first introduced for purely normal collisions. The extension to general collisions was then performed on the basis of physical arguments justifying decomposing an oblique collision into a normal and a tangential component. The ACTM was therefore supplemented with an additional model for tangential forces, the ATFM, which is the second main achievement of this paper. The strategy of the latter is to determine the required forces in an adapted way so that the desired motion is realized, such as vanishing relative motion of the contact point. The resulting entire model, termed the ACM, now is ready for use in very general settings.

In fact, a unifying concept underlying the different parts of the ACM can be extracted: forces are determined so as to fulfil physical requirements based on experimental knowledge. For the normal collision it is the restitution coefficient and for the tangential collision it is the relative tangential motion which are prescribed. This approach is inspired by the direct forcing applied in many IBM, where the difference between the actual velocity at a marker point and the desired velocity at that point steers the forcing term in the momentum equation. Currently, the strategy is being extended to more complex situations, such as particles of different shape.

https://doi.org/10.1017/jfm.2012.343 Published online by Cambridge University Press

The development of the ACM was thoroughly validated against experimental data in all the different steps, with very good results being obtained. It was also shown that the numerical cost of the new collision model is negligible in a large-scale simulation.

Stretching the collision process in time is an essential prerequisite in making large-scale simulations of highly loaded suspensions accessible. The paper hence provides a very simple, versatile and efficient model for normal and oblique collisions of spherical particles with and without rotation in viscous fluids which substantially improves upon existing models. Simulations assessing the performance of the new collision model for suspension-type flows with large numbers of particles are under way.

Acknowledgements

The present work was partially funded by DFG through grant Fr 1593/5-1. M. Uhlmann and C. Chan-Braun are acknowledged for stimulating discussions on IBM and particle-laden flows. W. Marth assisted in deriving the iterative scheme described in appendix A. G. Joseph and P. Gondret kindly provided their experimental data in electronic form.

Appendix A. Iterative determination of stiffness and damping in the ACTM

The numerical solution of (3.35) for a collision process is formally described here by

$$\mathcal{N}[\boldsymbol{K}] = \boldsymbol{S}, \tag{A 1}$$

where the operator $\mathcal{N}$ denotes an integration scheme, $\boldsymbol{K} = (d_n, k_n)^{\mathrm{T}}$ the desired unknowns, and $\boldsymbol{S} = (T_c, u_{out})^{\mathrm{T}}$ the state after collision where the distance $\zeta_n = 0$ is reached again.

For given collision time and rebound velocity, $\boldsymbol{S}^* = (T_c^*, u_{out}^*)^{\mathrm{T}}$, hence $\boldsymbol{K} = \boldsymbol{K}^*$ is sought such that

$$\tilde{\mathcal{N}}[\boldsymbol{K}^*] = \mathcal{N}[\boldsymbol{K}^*] - \boldsymbol{S}^* = 0. \tag{A 2}$$

A Newton scheme is used for the solution of the fixed-point problem (A 2):

$$\tilde{\mathcal{N}}[\boldsymbol{K}^{r+1}] = \tilde{\mathcal{N}}[\boldsymbol{K}^r] + \boldsymbol{J}[\tilde{\mathcal{N}}[\boldsymbol{K}^r]] \cdot \Delta\boldsymbol{K}^r \stackrel{!}{=} 0, \tag{A 3}$$

where r is the iteration counter and $\boldsymbol{J}$ the Jacobi matrix of $\tilde{\mathcal{N}}$ and

$$\Delta\boldsymbol{K}^r = \boldsymbol{K}^{r+1} - \boldsymbol{K}^r. \tag{A 4}$$

Equation (A 3) can be rewritten as an equation for the correction

$$\boldsymbol{J}[\tilde{\mathcal{N}}[\boldsymbol{K}^r]] \cdot \Delta\boldsymbol{K}^r = -\tilde{\mathcal{N}}[\boldsymbol{K}^r]. \tag{A 5}$$

Replacing $\tilde{N}[\boldsymbol{K}]$ with $\mathcal{N}[\boldsymbol{K}] - \boldsymbol{S}^*$ and using

$$\boldsymbol{J}[\tilde{\mathcal{N}}[\boldsymbol{K}]] = \boldsymbol{J}[\mathcal{N}[\boldsymbol{K}] - \boldsymbol{S}^*] = \boldsymbol{J}[\mathcal{N}[\boldsymbol{K}]], \tag{A 6}$$

yields the final equation for $\Delta\boldsymbol{K}^r$:

$$\boldsymbol{J}[\mathcal{N}[\boldsymbol{K}^r]] \cdot \Delta\boldsymbol{K}^r = -\mathcal{N}[\boldsymbol{K}^r] + \boldsymbol{S}^*. \tag{A 7}$$

Once the increment $\Delta\boldsymbol{K}^r$ is determined, $\boldsymbol{K}^{r+1}$ is obtained from (A 4). As a criterion to terminate iterations, the threshold $\boldsymbol{\epsilon} = |\boldsymbol{S}^* - \boldsymbol{S}| < 10^{-6}$ is used here. The numerical

https://doi.org/10.1017/jfm.2012.343 Published online by Cambridge University Press

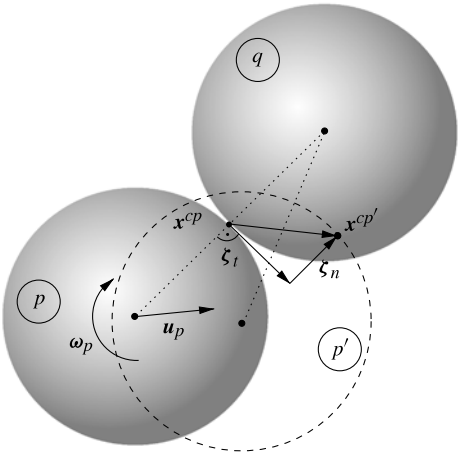


FIGURE 19. Normal overlapping $\boldsymbol{\zeta}_n$ and tangential elongation $\boldsymbol{\zeta}_t$ according to (4.15) for two colliding spheres p and q. The spheres drawn in solid mode represent the situation at the beginning of the contact with time $t = 0$. The broken circle with index p' denotes the position of particle p one time step later at $t' = t + \Delta t$ during the phase of contact with $0 < t' < T_c$. Particle q is supposed to be immobile for clarity.

solution of (A 1), required in each iteration, is performed by an explicit Runge–Kutta-scheme with small time steps and an adaptive time step control (Dahmen & Reusken 2008). In the standard Newton scheme, the Jacobi matrix is needed in each iteration step. To avoid its time-consuming computation, a quasi-Newton scheme is used here, replacing the Jacobi matrix by a Broyden approximation (Gay 1977).

Appendix B. Modification of the Cundall & Strack model for use with ACTM

Technical issues arise when realizing the concept of an accumulated elongation (4.15) in connection with long collision times, in particular when these are stretched by the ACTM. The contact point $\boldsymbol{x}^{cp}$ (figure 19) is defined as being midway between the particle centres during the contact phase, and the tangential plane goes through this point as illustrated in figure 15. The elongation of the spring in (4.15) is obtained by integration of the tangential relative velocity $\boldsymbol{g}_{t,pq}^{cp}$ at the contact point yielding the contact point $\boldsymbol{x}^{cp'}$ which is now disconnected from the normal and tangential directions (figure 19). With numerically overlapping particles the orientation of the tangential vector $\boldsymbol{t}$ changes in time during contact, so that $\boldsymbol{\zeta}_t \cdot \boldsymbol{n} \neq 0$ in general, i.e. $\boldsymbol{\zeta}_t$ has a contribution in the instantaneous normal direction.

When using the ACTM for the normal part of the collision, T_c is larger than the physical value and the coefficients in (3.35) are determined such that the rebound is still physically correct. If, however, the tangential model applied during the stretched contact generates a force in the normal direction the idea of the ACTM and the related optimization is spoiled. Hence the normal contribution is removed in the tangential model by subtraction, i.e.

$$\tilde{\boldsymbol{\zeta}}_t = \boldsymbol{\zeta}_t - (\boldsymbol{\zeta}_t \cdot \boldsymbol{n})\boldsymbol{n}, \tag{B 1}$$

which is then inserted instead of $\boldsymbol{\zeta}_t$ yielding

$$\boldsymbol{F}_t^{col} = -k_t \tilde{\boldsymbol{\zeta}}_t. \tag{B 2}$$

https://doi.org/10.1017/jfm.2012.343 Published online by Cambridge University Press

Appendix C. Alternative computation of tangential collision force

Instead of solving (4.22) in the body-fitted system another way for the computation of $\boldsymbol{F}_t^{col}$ directly in the laboratory system is proposed here. Using (3.6), (4.16) and (4.17), the relative surface velocity $\boldsymbol{g}_{pq}^{cp}$ at the new time level $t + \Delta t$ is given by

$$\boldsymbol{g}_{pq}^{cp} = \boldsymbol{A} \cdot \boldsymbol{F} + \boldsymbol{C}, \tag{C 1}$$

where the matrix $\boldsymbol{A}$ is written

$$\boldsymbol{A} = \frac{\Delta t}{I_p m_p} \times \begin{pmatrix} I_p(n_1^2 - 1) - m_p R_p^2(n_2^2 + n_3^2) & -n_1 n_2 (I_p + m_p R^2) & -n_1 n_3 (I_p + m_p R^2) \\ -n_1 n_2 (I_p + m_p R^2) & I_p(n_2^2 - 1) - m_p R_p^2(n_1^2 + n_3^2) & -n_2 n_3 (I_p + m_p R^2) \\ -n_1 n_3 (I_p + m_p R^2) & -n_2 n_3 (I_p + m_p R^2) & I_p(n_3^2 - 1) - m_p R_p^2(n_1^2 + n_2^2) \end{pmatrix} \tag{C 2}$$

and the vector $\boldsymbol{C}$ is

$$\boldsymbol{C} = \begin{pmatrix} u_p^1 - u_q^1 + n_3 R_p(\omega_p^2 + \omega_q^2) - n_2 R_p(\omega_p^3 + \omega_q^3) \\ u_p^2 - u_q^2 + n_1 R_p(\omega_p^3 + \omega_q^3) - n_3 R_p(\omega_p^1 + \omega_q^1) \\ u_p^3 - u_q^3 + n_2 R_p(\omega_p^1 + \omega_q^1) - n_1 R_p(\omega_p^2 + \omega_q^2) \end{pmatrix}. \tag{C 3}$$

Requiring that the relative surface velocity is zero amounts to imposing

$$\boldsymbol{A} \cdot \boldsymbol{F} + \boldsymbol{C} \stackrel{!}{=} 0. \tag{C 4}$$

The contact force $\boldsymbol{F}$ in (C 4) also may have components in the direction normal to the surface. To suppress the normal components, the contact force would have to fulfil the restriction

$$\boldsymbol{F} \cdot \boldsymbol{n} \stackrel{!}{=} 0. \tag{C 5}$$

With this condition, the desired contact force in the tangential direction is given by

$$\boldsymbol{F}_t = \boldsymbol{F}. \tag{C 6}$$

Equations (C 4)–(C 6) constitute an over-determined linear system with four equations and three unknowns:

$$\begin{pmatrix} a_{11} & a_{12} & a_{13} \\ a_{12} & a_{22} & a_{23} \\ a_{13} & a_{23} & a_{33} \\ n_1 & n_2 & n_3 \end{pmatrix} \cdot \begin{pmatrix} F_t^1 \\ F_t^2 \\ F_t^3 \end{pmatrix} = - \begin{pmatrix} C^1 \\ C^2 \\ C^3 \\ 0 \end{pmatrix} \tag{C 7}$$

abbreviated as

$$\boldsymbol{A}^* \cdot \boldsymbol{F}_t = \boldsymbol{C}^*. \tag{C 8}$$

Here, the linear least-squares solution $\boldsymbol{F}_t^{RMS}$ with

$$\| \boldsymbol{C}^* - \boldsymbol{A}^* \cdot \boldsymbol{F}_t^{RMS} \|_2 = \min \tag{C 9}$$

is computed and used further on. The numerical effort for the solution of (C 9) is extremely small compared to the cost of the fluid solver. The method (C 9) imposes $\boldsymbol{F}_t^{RMS}$ to be very close to tangential if $\|\boldsymbol{n}\| \gg \|\boldsymbol{A}\|$ with $\|.\|$ being a suitable norm. Since $m_p \propto R_p^3$ and $I_p \propto R_p^5$ (C 2) shows that $\boldsymbol{A} \propto R_p^{-3}$. Therefore, in the current

https://doi.org/10.1017/jfm.2012.343 Published online by Cambridge University Press

implementation $\boldsymbol{n}$ is replaced by $\boldsymbol{n}^* = \boldsymbol{n}/(I_p m_p)$, so that $\boldsymbol{n} \propto R_p^{-8}$. Hence, for $R_p \ll 1$, $\|\boldsymbol{n}\|$ is several orders of magnitude larger than $\|\boldsymbol{A}\|$ so that the force $\boldsymbol{F}_t^{RMS}$ being computed is the same as $\boldsymbol{F}_t^{col}$ according to (4.22) or (4.23) to 4 digits in the tests conducted.

REFERENCES

APOSTOLOU, K. & HRYMAK, A. 2008 Discrete element simulation of liquid-particle flows. *Comput. Chem. Engng* **32**, 841–856.

APTE, S. V., MARTIN, M. & PATANKAR, N. A. 2009 A numerical method for fully resolved simulation (FRS) of rigid particle-flow interactions in complex flows. *J. Comput. Phys.* **228**, 2712–2738.

ARDEKANI, A., DABIRI, S. & RANGEL, R. 2008 Collision of multi-particle and general shape objects in a viscous fluid. *J. Comput. Phys.* **227**, 10094–10107.

ARDEKANI, A. & RANGEL, R. H. 2008 Numerical investigation of particle–particle and particle–wall collisions in a viscous fluid. *J. Fluid Mech.* **596**, 437–466.

BARNOCKY, G. & DAVIS, R. 1988 Elastohydrodynamic collision and rebound of spheres: Experimental verification. *Phys. Fluids* **31**, 1324–1329.

BECKER, V. & BRIESEN, H. 2008 Tangential-force model for interactions between bonded colloidal particles. *Phys. Rev.* E **78**, 061404.

BRENNER, H. 1961 The slow motion of a sphere through a viscous fluid towards a plane surface. *Chem. Engng Sci.* **16**, 242–251.

CHAN-BRAUN, C., GARCÍA-VILLALBA, M. & UHLMANN, M. 2010 Numerical simulation of fully resolved particles in rough-wall turbulent open channel flow. In *7th International Conference on Multiphase Flows, Tampa, Florida, USA*, http://conferences.dce.ufl.edu/icmf2010/.

COX, R. & BRENNER, H. 1967 The slow motion of a sphere through a viscous fluid towards a plane surface. Small gap widths, including inertial effects. *Chem. Engng Sci.* **22**, 1753–1777.

CROWE, C. 2006 *Multiphase Flow Handbook*. CRC.

CROWE, C., SOMMERFELD, M. & TSUJI, Y. 1998 *Multiphase Flows with Droplets and Particles*. CRC.

CUNDALL, P. & STRACK, O. 1979 A discrete numerical model for granular assemblies. *Geotechnique* **29**, 47–65.

DAHMEN, W. & REUSKEN, A. 2008 *Numerik für Ingenieure und Naturwissenschaftler*. Springer.

DAVIS, R., RAGER, D. & GOOD, B. 2002 Elastohydrodynamic rebound of spheres from coated surfaces. *J. Fluid Mech.* **468**, 107–119.

DAVIS, R., SERAYSSOL, J. & HINCH, E. 1986 The elastohydrodynamic collision of two spheres. *J. Fluid Mech.* **163**, 479–497.

DIAZ-GOANO, C., MINEV, P. D. & NANDAKUMAR, K. 2003 A fictitious domain/finite element method for particulate flows. *J. Comput. Phys.* **192**, 105–123.

DONAHUE, C., HRENYA, C. & DAVIS, R. 2010*a* Stokes's cradle: Newton's cradle with liquid coating. *Phys. Rev. Lett.* **105**, 034501.

DONAHUE, C., HRENYA, C., DAVIS, R., NAKAGAWA, K., ZELINSKAYA, A. & JOSEPH, G. 2010*b* Stokes' cradle: normal three-body collisions between wetted particles. *J. Fluid Mech.* **650**, 479.

DONAHUE, C., HRENYA, C., ZELINSKAYA, A. & NAKAGAWA, K. J. 2008 Newton's cradle undone: experiments and collision models for the normal collision of three solid spheres. *Phys. Fluids* **20**, 113301.

EAMES, I. & DALZIEL, S. 2000 Dust resuspension by the flow around an impacting sphere. *J. Fluid Mech.* **403**, 305–328.

FENG, Z. & MICHAELIDES, E. 2005 Proteus: a direct forcing method in the simulations of particulate flows. *J. Comput. Phys.* **202**, 20–51.

FENG, Z., MICHAELIDES, E. & MAO, S. 2010 A three-dimensional resolved discrete particle method for studying particle–wall collision in a viscous fluid. *Trans. ASME: J. Fluids Engng* **132**, 091302.

https://doi.org/10.1017/jfm.2012.343 Published online by Cambridge University Press

FOERSTER, S., LOUGE, M., CHANG, H. & ALLIA, K. 1994 Measurements of the collision properties of small spheres. *Phys. Fluids* **6**, 1108–1115.

GAY, D. M. 1977 Some convergence properties of Broyden's method. *Working Paper 175*, National Bureau of Economic Research.

GLOWINSKI, R., PAN, T.-W., HESLA, T. & JOSEPH, D. 1999 A distributed Lagrange multiplier/fictitious domain method for particulate flows. *Intl J. Multiphase Flow* **25**, 755–794.

GLOWINSKI, R., PAN, T. W., HESLA, T. I., JOSEPH, D. D. & PRIAUX, J. 2001 A fictitious domain approach to the direct numerical simulation of incompressible viscous flow past moving rigid bodies: application to particulate flow. *J. Comput. Phys.* **169**, 363–426.

GOLDMAN, A., COX, R. & BRENNER, H. 1967 Slow viscous motion of a sphere parallel to a plane wall – Part I: motion through a quiescent fluid. *Chem. Engng Sci.* **22**, 637–651.

GONDRET, P., HALLOUIN, E., LANCE, M. & PETIT, L. 1999 Experiments on the motion of a solid sphere toward a wall: from viscous dissipation to elastohydrodynamic bouncing. *Phys. Fluids* **11**, 2803–2805.

GONDRET, P., LANCE, M. & PETIT, L. 2002 Bouncing motion of spherical particles in fluids. *Phys. Fluids* **14**, 643–652.

HAFF, P. & WERNER, B. 1986 Computer simulation of the mechanical sorting of grains. *Powder Technol.* **48**, 239–245.

HARLOW, F. H. & WELCH, J. E. 1965 Numerical calculation of time-dependent viscous incompressible flow of fluid with free surface. *Phys. Fluids* **8**, 2182–2189.

HERTZ, H. 1882 Über die Berührung fester elastischer Körper. *J. Reine Angew. Math.* **92**, 156–171.

HOOMANS, B. P. B., KUIPERS, J. A. M., BRIELS, W. J. & VAN SWAAIJ, W. P. M. 1996 Discrete particle simulation of bubble and slug formation in a two-dimensional gas-fluidised bed: a hard-sphere approach. *Chem. Engng Sci.* **51**, 99–108.

HU, H. H. 1996 Direct simulation of flows of solid–liquid mixtures. *Intl J. Multiphase Flow* **22**, 335–352.

HUNTER, S. 1957 Energy absorbed by elastic waves during impact. *J. Mech. Phys. Solids* **5**, 162–171.

IACCARINO, G. & VERZICCO, R. 2003 Immersed boundary technique for turbulent flow simulations. *Appl. Mech. Rev.* **56**, 331–347.

JOSEPH, G. 2003 Collisional dynamics of macroscopic particles in a viscous fluid. PhD thesis, California Institute of Technology, Pasadena, California.

JOSEPH, G. & HUNT, M. 2004 Oblique particle wall collisions in a liquid. *J. Fluid Mech.* **510**, 71–93.

JOSEPH, G., ZENIT, R., HUNT, M. & ROSENWINKEL, A. 2001 Particle wall collisions in a viscous fluid. *J. Fluid Mech.* **433**, 329–346.

KEMPE, T. & FRÖHLICH, J. 2012 An improved immersed boundary method with direct forcing for the simulation of particle laden flows. *J. Comput. Phys.* **231**, 3663–3684.

KHARAZ, A. H., GORHAM, D. A. & SALMAN, A. D. 1999 Accurate measurement of particle impact parameters. *Meas. Sci. Technol.* **10**, 31–35.

KHARAZ, A. H., GORHAM, D. A. & SALMAN, A. D. 2001 An experimental study of the elastic rebound of spheres. *Powder Technol.* **120**, 281–291.

KRUGGEL-EMDEN, H., SIMSEK, E., RICKELT, S., WIRTZ, S. & SCHERER, V. 2007 Review and extension of normal force models for the discrete element method. *Powder Technol.* **171**, 157–173.

KRUGGEL-EMDEN, H., WIRTZ, S. & SCHERER, V. 2008 A study on tangential force laws applicable to the discrete element method (DEM) for materials with viscoelastic or plastic behaviour. *Chem. Engng Sci.* **63**, 1523–1541.

LADD, A. 1997 Sedimentation of homogeneous suspensions of non-Brownian spheres. *Phys. Fluids* **9**, 491–499.

LAIN, S., SOMMERFELD, M. & KUSSIN, J. 2002 Experimental studies and modelling of four-way coupling in particle-laden horizontal channel flow. *Intl J. Heat Fluid Flow* **23**, 647–656.

LEGENDRE, D., ZENIT, R., DANIEL, C. & GUIRAUD, P. 2006 A note on the modelling of the bouncing of spherical drops or solid spheres on a wall in viscous fluid. *Chem. Engng Sci.* **61**, 3543–3549.

https://doi.org/10.1017/jfm.2012.343 Published online by Cambridge University Press

LEOPARDI, P. 2006 A partition of the unit sphere into regions of equal area and small diameter. *Electron. Trans. Numer. Anal.* **25**, 309–327.

LEWEKE, T., THOMPSON, M. & HOURIGAN, K. 2004 Vortex dynamics associated with the collision of a sphere with a wall. *Phys. Fluids* **16**, L74–L77.

LEWEKE, T., THOMPSON, M. & HOURIGAN, K. 2006 Instability of the flow around an impacting sphere. *J. Fluids Struct.* **22**, 961–971.

LORENZ, A., TUOZZOLO, C. & LOUGE, M. Y. 1997 Measurements of impact properties of small, nearly spherical particles. *Exp. Mech.* **37**, 292–298.

LUN, C. & SAVAGE, S. 1987 A simple kinetic theory for granular flow of rough, inelastic, spherical particles. *J. Appl. Mech.* **54**, 47–53.

MAW, N., BARBER, J. & FAWCETT, J. 1976 The oblique impact of elastic spheres. *Wear* **38**, 101–114.

MAW, N., BARBER, J. & FAWCETT, J. 1977 The rebound of elastic bodies in oblique contact. *Mech. Res. Comm.* **4**, 17–22.

MCLAUGHLIN, M. 1968 An experimental study of particle–wall collision relating to flow of solid particles in fluid. Master's thesis, California Institute of Technology, Pasadena, California.

MINDLIN, R. 1949 Compliance of elastic bodies in contact. *J. Appl. Mech.* **16**, 259–268.

MINDLIN, R. & DERESIEWICZ, H. 1953 Elastic spheres in contact under varying oblique forces. *J. Appl. Mech.* **20**, 327–344.

MITTAL, R. & IACCARINO, G. 2005 Immersed boundary methods. *Annu. Rev. Fluid Mech.* **37**, 239–261.

MOHD-YUSOF, J. 1997 Combined immersed boundary/B-Spline method for simulations of flows in complex geometries. *Center for Turbulence Research. Annual Research Briefs. NASA Ames/Stanford University*, pp. 317–327.

NGUYEN, N. & LADD, A. 2002 Lubrication corrections for lattice-Boltzmann simulations of particle suspensions. *Phys. Rev.* E **66**, 046708.

PAN, T. & GLOWINSKI, R. 2002 Direct simulation of the motion of neutrally buoyant circular cylinders in plane poiseuille flow. *J. Comput. Phys.* **181**, 260–279.

PAPISTA, E., DIMITRAKIS, D. & YIANTSIOS, S. G. 2011 Direct numerical simulation of incipient sediment motion and hydraulic conveying. *Ind. Engng Chem. Res.* **50**, 630–638.

PESKIN, C. 1977 Numerical analysis of blood flow in the heart. *J. Comput. Phys.* **25**, 220–252.

PIANET, G., TEN CATE, A., DERKSEN, J. & ARQUIS, E. 2007 Assessment of the 1-fluid method for DNS of particulate flows: sedimentation of a single sphere at moderate to high Reynolds numbers. *Comput. Fluids* **36**, 359–375.

POPOV, V. & PSAKHIE, S. 2007 Numerical simulation methods in tribology. *Tribol. Intl* **40**, 916–923.

PÖSCHEL, T. & SCHWAGER, T. 2005 *Computational Granular Dynamics: Models and Algorithms*. Springer.

PROKUNIN, A. & WILLIAMS, M. 1996 Spherical particle sedimentation along an inclined plane at high Reynolds numbers. *Fluid Dyn.* **31**, 567–572.

PROKUNIN, A. N. 1998 Spherical particle sedimentation along an inclined plane at small Reynolds numbers. *Fluid Dyn.* **23**, 573–579.

PROSPERETTI, A. & TRYGGVASON, G. 2007 *Computational Methods for Multiphase Flow*. Cambridge University Press.

REED, J. 1985 Energy losses due to elastic wave propagation during an elastic impact. *J. Phys.* D: *Appl. Phys.* **18**, 2329–2337.

ROMA, A. M., PESKIN, C. S. & BERGER, M. J. 1999 An adaptive version of the immersed boundary method. *J. Comput. Phys.* **153**, 509–534.

SCHILLER, L. & NAUMANN, Z. 1933 Über die grundlegenden berechnungen bei der schwerkraftaufbereitung. *Z. Ver. Dtsch. Ing.* 318–338.

SCHWARZER, S. 1995 Sedimentation and flow through porous media: simulating dynamically coupled discrete and continuum phases. *Phys. Rev.* E **52**, 6461–6475.

STEVENS, A. & HRENYA, C. 2005 Comparison of soft-sphere models to measurements of collision properties during normal impacts. *Powder Technol.* **154**, 99–109.

https://doi.org/10.1017/jfm.2012.343 Published online by Cambridge University Press

SUNDARAM, S. & COLLINS, L. 1999 A numerical study of the modulation of isotropic turbulence by suspended particles. *J. Fluid Mech.* **379**, 105–143.

TEN CATE, A., DERKSEN, J. J., PORTELA, L. M. & VAN DEN AKKER, H. E. A. 2004 Fully resolved simulations of colliding monodisperse spheres in forced isotropic turbulence. *J. Fluid Mech.* **519**, 233–271.

TEN CATE, A., NIEUWSTAD, C., DERKSEN, J. & DEN AKKER, H. V. 2002 Particle imaging velocimetry experiments and lattice-Boltzmann simulations on a single sphere settling under gravity. *Phys. Fluids* **14**, 4012–4025.

THOMPSON, M., LEWEKE, T. & HOURIGAN, K. 2007 Sphere-wall collisions: vortex dynamics and stability. *J. Fluid Mech.* **575**, 121–148.

TIMOSHENKO, S. & GOODIER, J. 1970 *Theory of Elasticity*. McGraw-Hill.

TRYGGVASON, G., THOMAS, S., LU, J., ABOULHASANZADEH, B. & TSENGUE, V. 2010 Multiscale computation of multiphase flows. In *7th International Conference on Multiphase Flows, Tampa, Florida, USA*.

UHLMANN, M. 2005 An immersed boundary method with direct forcing for the simulation of particulate flows. *J. Comput. Phys.* **209**, 448–476.

UHLMANN, M. 2008 Interface-resolved direct numerical simulation of vertical particulate channel flow in the turbulent regime. *Phys. Fluids* **20**, 053305.

UZGOREN, E., SINGH, R., SIM, J. & SHYY, W. 2007 Computational modelling for multiphase flows with spacecraft application. *Prog. Aerosp. Sci.* **43**, 138–192.

VANELLA, M. & BALARAS, E. 2009 A moving-least-squares reconstruction for embedded-boundary formulations. *J. Comput. Phys.* **228**, 6617–6628.

VEERAMANI, C., MINEV, P. & NANDAKUMAR, K. 2009 Collision modelling between two non-Brownian particles in multiphase flow. *Intl J. Therm. Sci.* **48**, 226–233.

VOWINCKEL, B., KEMPE, T. & FRÖHLICH, 2011 Impact of collision models on particle transport in open channel flow. In *7th International Symposium on Turbulence and Shear Flow Phenomena. Ottawa, Canada*.

VU-QUOC, L., LESBURG, L. & ZHANG, X. 2004 An accurate tangential force–displacement model for granular-flow simulations: contacting spheres with plastic deformation, force-driven formulation. *J. Comput. Phys.* **196**, 298–326.

WALTON, O. & BRAUN, R. 1986 Viscosity, granular-temperature, and stress calculations for shearing assemblies of inelastic, frictional disks. *J. Rheol.* **30**, 949–980.

WALTON, O. R. 1993 Particulate two-phase flow. In *Numerical Simulation of Inelastic, Frictional Particle–particle Interactions*, pp. 884–911. Butterworth-Heinemann.

WAN, D. & TUREK, S. 2006 Direct numerical simulation of particulate flow via multigrid FEM techniques and the fictitious boundary method. *Intl J. Numer. Meth. Fluids* **51**, 531–566.

XU, B. & YU, A. 1997 Numerical simulation of the gas–solid flow in a fluidized bed by combining discrete particle method with computational fluid dynamics. *Chem. Engng Sci.* **52**, 2785–2809.

YANG, C., YORK, D. & BROECKX, W. 2008 Numerical simulation of sedimentation of microparticles using the discrete particle method. *Particuology* **6**, 38–49.

YANG, F. & HUNT, M. 2006 Dynamics of particle–particle collisions in a viscous liquid. *Phys. Fluids* **18**, 121506.

YANG, L., SEDDON, J., MULLIN, T., DEL PINO, C. & ASHMORE, J. 2006 The motion of a rough particle in a Stokes flow adjacent to a boundary. *J. Fluid Mech.* **557**, 337–346.

ZENIT, R. & HUNT, M. 1999 Mechanics of immersed particle collisions. *Trans. ASME: J. Fluids Engng* **121**, 179–184.

ZHANG, J., FAN, L., ZHU, C., PFEFFER, R. & QI, D. 1999 Dynamic behaviour of collision of elastic spheres in viscous fluids. *Powder Technol.* **106**, 98–109.

https://doi.org/10.1017/jfm.2012.343 Published online by Cambridge University Press